
Intra Order-Preserving Functions for Calibration of Multi-Class Neural Networks

Amir Rahimi*
ANU, ACRV
amir.rahimi@anu.edu.au

Amirreza Shaban*
Georgia Tech
ashaban@uw.edu

Ching-An Cheng*
Microsoft Research
chinganc@microsoft.com

Richard Hartley
Google Research, ANU, ACRV
richard.hartley@anu.edu.au

Byron Boots
University of Washington
bboots@cs.washington.edu

Abstract

Predicting calibrated confidence scores for multi-class deep networks is important for avoiding rare but costly mistakes. A common approach is to learn a post-hoc calibration function that transforms the output of the original network into calibrated confidence scores while maintaining the network’s accuracy. However, previous post-hoc calibration techniques work only with simple calibration functions, potentially lacking sufficient representation to calibrate the complex function landscape of deep networks. In this work, we aim to learn general post-hoc calibration functions that can preserve the top- k predictions of any deep network. We call this family of functions *intra order-preserving* functions. We propose a new neural network architecture that represents a class of intra order-preserving functions by combining common neural network components. Additionally, we introduce *order-invariant* and *diagonal* sub-families, which can act as regularization for better generalization when the training data size is small. We show the effectiveness of the proposed method across a wide range of datasets and classifiers. Our method outperforms state-of-the-art post-hoc calibration methods, namely temperature scaling and Dirichlet calibration, in several evaluation metrics for the task.

1 Introduction

Deep neural networks have demonstrated impressive accuracy in classification tasks, such as image recognition [8, 28] and medical research [10, 3]. These exciting results have recently motivated engineers to adopt deep networks as default components in building decision systems; for example, a multi-class neural network can be treated as a probabilistic predictor and its softmax output can provide the confidence scores of different actions for the downstream decision making pipeline [6, 2, 21]. While this is an intuitive idea, recent research has found that deep networks, despite being accurate, can be overconfident in their predictions, exhibiting high calibration error [20, 7, 11]. In other words, trusting the network’s output naively as confidence scores in system design could cause undesired consequences: a serious issue for applications where mistakes are costly, such as medical diagnosis and autonomous driving.

A promising approach to address the miscalibration is to augment a given network with a parameterized calibration function, such as extra learnable layers. This additional component is tuned post-hoc using a held-out calibration dataset, so that the effective full network becomes calibrated [7, 14, 16, 15, 27, 35]. In contrast to usual deep learning, the calibration dataset here is typically

*Equal Contribution.

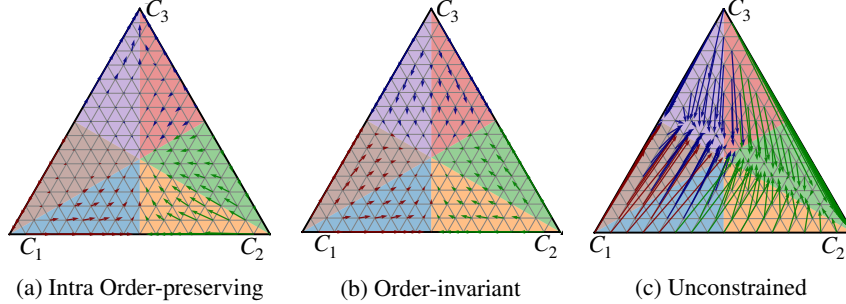


Figure 1: Comparing instances of intra order-preserving and order-invariant family defined on the 2-dimensional unit simplex. Points $C_1 = [1, 0, 0]^T$, $C_2 = [0, 1, 0]^T$, $C_3 = [0, 0, 1]^T$ are the simplex corners. Arrows depict how an input is mapped by each function. Unconstrained function freely maps the input probabilities, intra order-preserving function enforces the outputs to stay within the same colored region as the inputs, and order-invariant function further enforces the vector fields to be the same among all the 6 colored regions as reflected in the symmetry in the visualization.

small. Therefore, learning an overly general calibration function can easily overfit and actually reduce the accuracy of the given network [7, 14]. Careful design regularization and parameterization of calibration functions is imperative.

A classical non-parametric technique is isotonic regression [36], which learns a monotonic staircase calibration function with minimal change in the accuracy. But the complexity of non-parametric learning can be too expensive to provide the needed generalization [16, 15]. By contrast, Guo *et al.* [7] proposed to learn a scalar parameter to rescale the original output logits, at the cost of being suboptimal in calibration [20]; see also Section 6. Recently, Kull *et al.* [14] proposed to learn linear transformations of the output logits. While this scheme is more expressive than the temperature scaling above, it does not explore non-linear calibration functions.

In general, a preferable hypothesis space needs to be expressive and, at the same time, provably preserve the accuracy of any given network it calibrates. Limiting the expressivity of calibration functions can be an issue, especially when calibrating deep networks with complicated landscapes.

The main contribution of this paper is introducing a learnable space of functions, called *intra order-preserving* family. Informally speaking, an intra order-preserving function $f : \mathbb{R}^n \rightarrow \mathbb{R}^n$ is a vector-valued function whose output values always share the same ordering as the input values across the n dimensions. For example, if $\mathbf{x} \in \mathbb{R}^n$ is increasing from coordinate 1 to n , then so is $f(\mathbf{x})$. In addition, we introduce order-invariant and diagonal structures, which utilize the shared characteristics between different input dimensions to improve generalization. For illustration, we depict instances of 3-dimensional intra order-preserving and order-invariant functions defined on the unit simplex and compare them to an unconstrained function in Fig. 1. We use arrows to show how inputs on the simplex are mapped by each function. Each colored subset in the simplex denotes a region with the same input order; for example, we have $x_3 > x_2 > x_1$ inside the red region where the subscript i denotes the i th element of a vector. For the intra order-preserving function shown in Fig. 1a arrows stay within the same colored region as the inputs, but the vector fields in two different colored region are independent to each other. Order-invariant function in Fig. 1b further keeps the function permutation invariant, enforcing the vector fields to be the same among all the 6 colored regions (as reflected in the symmetry in Fig. 1b). This property of order-preserving functions significantly reduce the hypothesis space in learning, from the functions on whole simplex to functions on one colored region, for better generalization.

We identify necessary and sufficient conditions for describing intra order-preserving functions, study their differentiability, and propose a novel neural network architecture that can represent complex intra order-preserving function through common neural network components. From practical point of view, we devise a new post-hoc network confidence calibration technique using different intra order-invariant sub-families. Because a post-hoc calibration function keeps the top- k class prediction *if and only if* it is an intra order-preserving function, learning the post-hoc calibration function within the intra order-preserving family presents a solution to the dilemma between accuracy and flexibility faced in the previous approaches. We conduct several experiments to validate the benefits of learning

with these new functions for post-hoc network calibration. The results demonstrate improvement over various calibration performance metrics, compared with the original network, temperature scaling [7], and Dirichlet calibration [14].

2 Problem Setup

We address the problem of calibrating neural networks for n -class classification. Let define $[n] := \{1, \dots, n\}$, $\mathcal{Z} \subseteq \mathbb{R}^d$ be the domain, $\mathcal{Y} = [n]$ be the label space, and let Δ_n denote the $n - 1$ dimensional unit simplex. Suppose we are given a trained probabilistic predictor $\phi_o : \mathbb{R}^d \rightarrow \Delta_n$ and a small calibration dataset \mathcal{D}_c of i.i.d. samples drawn from an unknown distribution π on $\mathcal{Z} \times \mathcal{Y}$. For simplicity of exposition, we assume that ϕ_o can be expressed as the composition $\phi_o =: \mathbf{sm} \circ \mathbf{g}$, with $\mathbf{g} : \mathbb{R}^d \rightarrow \mathbb{R}^n$ being a non-probabilistic n -way classifier and $\mathbf{sm} : \mathbb{R}^n \rightarrow \Delta_n$ being the softmax operator², i.e. $\mathbf{sm}_i(\mathbf{x}) = \frac{\exp(\mathbf{x}_i)}{\sum_{j=1}^n \exp(\mathbf{x}_j)}$, for $i \in \mathcal{Y}$, where the subscript i denotes the i th element of a vector. When queried at $\mathbf{z} \in \mathcal{Z}$, the probabilistic predictor ϕ_o returns $\arg \max_i \phi_{o,i}(\mathbf{z})$ as the predicted label and $\max_i \phi_{o,i}(\mathbf{z})$ as the associated confidence score. (The top- k prediction is defined similarly.) We say $\mathbf{g}(\mathbf{z})$ is the *logits* of \mathbf{z} with respect to ϕ_o .

Given ϕ_o and \mathcal{D}_c , our goal is to learn a post-hoc calibration function $\mathbf{f} : \mathbb{R}^n \rightarrow \mathbb{R}^n$ such that the new probabilistic predictor $\phi := \mathbf{sm} \circ \mathbf{f} \circ \mathbf{g}$ is better calibrated *and* keeps the accuracy (or similar performance concepts like top- k accuracy) of the original network ϕ_o . That is, we want to learn new logits $\mathbf{f}(\mathbf{g}(\mathbf{z}))$ of \mathbf{z} . As we will discuss, this task is non-trivial, because while learning \mathbf{f} might improve calibration, doing so could also risk over-fitting to the small dataset \mathcal{D}_c and damaging accuracy. To make this statement more precise, below we first review the definition of perfect calibration [7] and common calibration metrics and then discuss challenges in learning \mathbf{f} with \mathcal{D}_c .

Definition 1. For a distribution π on $\mathcal{Z} \times \mathcal{Y}$ and a probabilistic predictor $\psi : \mathbb{R}^d \rightarrow \Delta_n$, let random variables $\mathbf{z} \in \mathcal{Z}$, $y \in \mathcal{Y}$ be distributed according to π , and define random variables $\hat{y} := \arg \max_i \psi_i(\mathbf{z})$ and $\hat{p} := \psi_{\hat{y}}(\mathbf{z})$. We say ψ is *perfectly calibrated* with respect to π , if for any $p \in [0, 1]$, it satisfies $\text{Prob}(\hat{y} = y | \hat{p} = p) = p$.

Note that \mathbf{z} , y , \hat{y} and \hat{p} are correlated random variables. Therefore, Definition 1 essentially means that, if ψ is perfectly calibrated, then for any $p \in [0, 1]$, the true label y and the predicted label \hat{y} match, with a probability exactly p in the events where \mathbf{z} satisfies $\max_i \psi_i(\mathbf{z}) = p$.

In practice, learning a perfectly calibrated predictor is unrealistic, so we need a way to measure the calibration error. A common calibration metric is called Expected Calibration Error (ECE) [23]: $\text{ECE} = \sum_{m=1}^M \frac{|B_m|}{N} |\text{acc}(B_m) - \text{conf}(B_m)|$. This equation is calculated in two steps: First the confidence scores of samples in \mathcal{D}_c are partitioned into M equally spaced bins $\{B_m\}_{m=1}^M$. Second the weighted average of the differences between the average confidence $\text{conf}(B_m) = \frac{1}{|B_m|} \sum_{i \in B_m} \hat{p}^i$ and the accuracy $\text{acc}(B_m) = \frac{1}{|B_m|} \sum_{i \in B_m} \mathbb{1}(y^i = \hat{y}^i)$ in each bin is computed as the ECE metric, where $|B_m|$ denotes the size of bin B_m , $\mathbb{1}$ is the indicator function, and the superscript i indexes the sampled random variable. In addition to ECE, other calibration metrics have also been proposed [7, 25, 1, 17]; e.g., Classwise-ECE [14] and Brier score [1] are proposed as measures of classwise-calibration. All the metrics for measuring calibration have their own pros and cons. Here, we consider the most commonly used metrics for measuring calibration and leave their analysis for future work.

While the calibration metrics above measure the deviation from perfect calibration in Definition 1, they are usually not suitable loss functions for optimizing neural networks, e.g., due to the lack of continuity or non-trivial computation time. Instead, the calibration function \mathbf{f} in $\phi = \mathbf{sm} \circ \mathbf{f} \circ \mathbf{g}$ is often optimized indirectly through a surrogate loss function (e.g. the negative log-likelihood) defined on the held-out calibration dataset \mathcal{D}_c [7].

2.1 Importance of Inductive Bias

Unlike regular deep learning scenarios, here the calibration dataset \mathcal{D}_c is relatively small. Therefore, controlling the capacity of the hypothesis space of \mathbf{f} becomes a crucial topic [7, 15, 14]. There is typically a trade-off between preserving accuracy and improving calibration: Learning \mathbf{f} could

²The softmax requirement is not an assumption but for making the notation consistent with the literature. The proposed algorithm can also be applied to the output of general probabilistic predictors.

improve the calibration performance, but it could also change the decision boundary of ϕ from ϕ_o decreasing the accuracy. While using simple calibration functions may be applicable when ϕ_o has a simple function landscape or is already close to being well calibrated, such a function class might not be sufficient to calibrate modern deep networks with complex decision boundaries as we will show in the experiments in Section 6.

The observation above motivates us to investigate the possibility of learning calibration functions within a hypothesis space that can provably guarantee preserving the accuracy of the original network ϕ_o . The identification of such functions would address the previous dilemma and give precisely the needed structure to ensure generalization of calibration when the calibration dataset \mathcal{D}_c is small.

3 Intra Order-Preserving Functions

In this section, we formally describe this desirable class of functions for post-hoc network calibration. We name them *intra order-preserving functions*. Learning within this family is both necessary and sufficient to keep the top- k accuracy of the original network unchanged. We also study additional function structures on this family (e.g. limiting how different dimensions can interact), which can be used as regularization in learning calibration functions. Last, we discuss a new neural network architecture for representing these functions.

3.1 Setup: Sorting and Ranking

We begin by defining sorting functions and ranking in preparation for the formal definition of intra order-preserving functions. Let $\mathbb{P}^n \subset \{0, 1\}^{n \times n}$ denote the set of $n \times n$ permutation matrices. Sorting can be viewed as a permutation matrix; Given a vector $\mathbf{x} \in \mathbb{R}^n$, we say $S : \mathbb{R}^n \rightarrow \mathbb{P}^n$ is a *sorting function* if $\mathbf{y} = S(\mathbf{x})\mathbf{x}$ satisfies $y_1 \geq y_2 \geq \dots \geq y_n$. In case there are ties in the input vector \mathbf{x} , the sorting matrix can not be uniquely defined. To resolve this, we use a pre-defined *tie breaker* vector which is used as a tie breaking protocol. We say a vector $\mathbf{t} \in \mathbb{R}^n$ is a tie breaker if $\mathbf{t} = P\mathbf{r}$, for some $P \in \mathbb{P}^n$, where $\mathbf{r} = [1, \dots, n]^T \in \mathbb{R}^n$. Tie breaker pre-assigns priorities to indices of the input vector and is used to resolve ties. For instance, $\mathbf{S}_1 = \begin{bmatrix} 1 & 0 \\ 0 & 1 \end{bmatrix}$ and $\mathbf{S}_2 = \begin{bmatrix} 0 & 1 \\ 1 & 0 \end{bmatrix}$ are the unique sorting matrices of input $\mathbf{x} = [0, 0]^T$ with respect to tie breaker $\mathbf{t}_1 = [1, 2]^T$ and $\mathbf{t}_2 = [2, 1]^T$, respectively. We say two vectors $\mathbf{u}, \mathbf{v} \in \mathbb{R}^n$ *share the same ranking* if $S(\mathbf{u}) = S(\mathbf{v})$ for any tie breaker \mathbf{t} .

3.2 Intra Order-Preserving Functions

We define the *intra order-preserving* property with respect to different coordinates of a vector input.

Definition 2. We say a function $\mathbf{f} : \mathbb{R}^n \rightarrow \mathbb{R}^n$ is *intra order-preserving*, if, for any $\mathbf{x} \in \mathbb{R}^n$, both \mathbf{x} and $\mathbf{f}(\mathbf{x})$ share the same ranking.

The output of an intra order-preserving function $\mathbf{f}(\mathbf{x})$ maintains *all* ties and strict inequalities between elements of the input vector \mathbf{x} . Namely, for all $i, j \in [n]$, we have $x_i > x_j$ (or $x_i = x_j$) if and only if $f_i(\mathbf{x}) > f_j(\mathbf{x})$ (or $f_i(\mathbf{x}) = f_j(\mathbf{x})$). For example, a simple intra order-preserving function is the temperature scaling $\mathbf{f}(\mathbf{x}) = \mathbf{x}/t$ for some $t > 0$. Another common instance is the softmax operator.

Clearly, applying an intra order-preserving function as the calibration function in $\phi = \mathbf{sm} \circ \mathbf{f} \circ \mathbf{g}$ does not change top- k predictions between ϕ and $\phi_o = \mathbf{sm} \circ \mathbf{g}$.

Next, we provide a necessary and sufficient condition for constructing continuous, intra order-invariant functions. This theorem will be later used to design neural network architectures for learning calibration functions. Note that for a vector $\mathbf{v} \in \mathbb{R}^n$ and an upper-triangular matrix of ones U , $U\mathbf{v}$ is the *reverse* cumulative sum of \mathbf{v} (i.e. $(U\mathbf{v})_i = \sum_{j=i}^n v_j$).

Theorem 1. A continuous function $\mathbf{f} : \mathbb{R}^n \rightarrow \mathbb{R}^n$ is *intra order-preserving*, if and only if $\mathbf{f}(\mathbf{x}) = S(\mathbf{x})^{-1}U\mathbf{w}(\mathbf{x})$ with U being an upper-triangular matrix of ones and $\mathbf{w} : \mathbb{R}^n \rightarrow \mathbb{R}^n$ being a continuous function such that

- $w_i(\mathbf{x}) = 0$, if $y_i = y_{i+1}$ and $i < n$,
- $w_i(\mathbf{x}) > 0$, if $y_i > y_{i+1}$ and $i < n$,
- $w_n(\mathbf{x})$ is arbitrary,

where $\mathbf{y} = S(\mathbf{x})\mathbf{x}$ is the sorted version of \mathbf{x} .

The proof is deferred to Appendix. Here we provide as sketch as to why Theorem 1 is true. Since $w_i(\mathbf{x}) \geq 0$ for $i < n$, applying the matrix U on $\mathbf{w}(\mathbf{x})$ results in a sorted vector $U\mathbf{w}(\mathbf{x})$. Thus, applying $S(\mathbf{x})^{-1}$ further on $U\mathbf{w}(\mathbf{x})$ makes sure that $\mathbf{f}(\mathbf{x})$ has the same ordering as the input vector \mathbf{x} . The reverse direction can be proved similarly. For the continuity, observe that the sorting function $S(\mathbf{x})$ is piece-wise constant with discontinuities only when there is a tie in the input \mathbf{x} . This means that if the corresponding elements in $U\mathbf{w}(\mathbf{x})$ are also equally valued when a tie happens, the discontinuity of the sorting function S does not affect the continuity of \mathbf{f} inherited from \mathbf{w} .

3.3 Order-invariant and Diagonal Sub-families

Different classes in a classification task typically have shared characteristics. Therefore, calibration functions sharing properties across different classes can work as a suitable inductive bias in learning. Here we use this idea to define two additional structures interesting to intra order-preserving functions: *order-invariant* and *diagonal* properties. Similar to the purpose of the previous section, we will study necessary and sufficient conditions for functions with these properties.

First, we study the concept of order-invariant functions.

Definition 3. We say a function $\mathbf{f} : \mathbb{R}^n \rightarrow \mathbb{R}^n$ is *order-invariant*, if $\mathbf{f}(P\mathbf{x}) = P\mathbf{f}(\mathbf{x})$ for all $\mathbf{x} \in \mathbb{R}^n$ and permutation matrices $P \in \mathbb{P}^n$.

For an order-invariant function \mathbf{f} , when two elements \mathbf{x}_i and \mathbf{x}_j in the input \mathbf{x} are swapped, the corresponding elements $\mathbf{f}_i(\mathbf{x})$ and $\mathbf{f}_j(\mathbf{x})$ in the output $\mathbf{f}(\mathbf{x})$ are also swapped. In this way, the mapping learned for the i th class can also be used for the j th class. Thus, the order-invariant family shares the calibration function between different classes while allowing the output of each class be a function of all other class predictions.

We characterize in the theorem below the properties of functions that are both intra order-preserving and order-invariant (an instance is the softmax operator). It shows that, to make an intra order-preserving function also order-invariant, we just need to feed the function \mathbf{w} in Theorem 1 with the sorted input $\mathbf{y} = S(\mathbf{x})\mathbf{x}$ instead of \mathbf{x} . This scheme makes the learning of \mathbf{w} easier since it always sees sorted vectors (which are a subset of \mathbb{R}^n).

Theorem 2. A continuous, intra order-preserving function $\mathbf{f} : \mathbb{R}^n \rightarrow \mathbb{R}^n$ is order-invariant, if and only if $\mathbf{f}(\mathbf{x}) = S(\mathbf{x})^{-1}U\mathbf{w}(\mathbf{y})$, where U , \mathbf{w} , and \mathbf{y} are in Theorem 1.

Another structure of interest here is the diagonal property.

Definition 4. We say a function $\mathbf{f} : \mathbb{R}^n \rightarrow \mathbb{R}^n$ is *diagonal*, if $\mathbf{f}(\mathbf{x}) = [f_1(\mathbf{x}_1), \dots, f_n(\mathbf{x}_n)]$ for $f_i : \mathbb{R} \rightarrow \mathbb{R}$ with $i \in [n]$.

In the context of calibration, a diagonal calibration function means that different class predictions do not interact with each other in \mathbf{f} . Defining diagonal family is mostly motivated by the success of temperature scaling method [7], which is a linear diagonal intra order-preserving function. Therefore, although diagonal intra order-preserving functions may sound limiting in learning calibration functions, they still represent a useful class of functions.

The next theorem relates diagonal intra order-preserving functions to increasing functions.

Theorem 3. A continuous, intra order-preserving function $\mathbf{f} : \mathbb{R}^n \rightarrow \mathbb{R}^n$ is diagonal, if and only if $\mathbf{f}(\mathbf{x}) = [\bar{f}(\mathbf{x}_1), \dots, \bar{f}(\mathbf{x}_n)]$ for some continuous and increasing function $\bar{f} : \mathbb{R} \rightarrow \mathbb{R}$.

Compared with general diagonal functions, diagonal intra order-preserving automatically implies that the same function \bar{f} is shared across all dimensions. Thus, learning with diagonal intra order-preserving functions benefits from parameter-sharing across different dimensions, which could drastically decrease the number of parameters.

Finally, below we show that functions in this sub-family are also order-invariant and inter order-preserving. Note that inter and intra order-preserving are orthogonal definitions. Inter order-preserving is also an important property for calibration functions, since this property guarantees that $\mathbf{f}_i(\mathbf{x})$ increases with the original class logit \mathbf{x}_i . The set diagram in Fig. 2 depicts the relationship among different intra order-preserving families.

Definition 5. We say a function $\mathbf{f} : \mathbb{R}^m \rightarrow \mathbb{R}^n$ is *inter order-preserving* if, for any $\mathbf{x}, \mathbf{y} \in \mathbb{R}^m$ such that $\mathbf{x} \geq \mathbf{y}$, $\mathbf{f}(\mathbf{x}) \geq \mathbf{f}(\mathbf{y})$, where \geq denotes elementwise comparison.

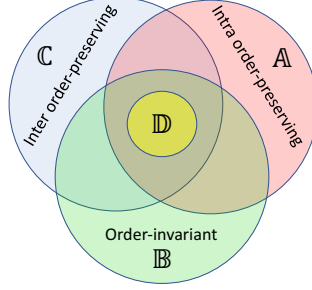


Figure 2: Relationship between different function families. Theorem 1 specifies the intra order-preserving functions \mathbb{A} . Theorem 2 specifies the intra order-preserving and order-invariant functions $\mathbb{A} \cap \mathbb{B}$. Theorem 3 specifies the diagonal intra order-preserving functions \mathbb{D} . By Corollary 1, these functions are also order-invariant and inter order-preserving i.e. $\mathbb{D} \subseteq \mathbb{A} \cap \mathbb{B} \cap \mathbb{C}$.

Corollary 1. *A diagonal, intra order-preserving function is order-invariant and inter order-preserving*

3.4 Practical Considerations

Theorems 1 and 2 describe general representations of intra order-preserving functions through a function \mathbf{w} that satisfies certain non-negative constraints. Inspired by these theoretical results, we propose a neural network architecture, Fig. 3, to represent exactly a family of intra order-preserving functions.

The main idea in Fig. 3 is to parameterize \mathbf{w} through a composition of smaller functions. For $i < n$, we set $\mathbf{w}_i(\mathbf{x}) = \sigma(\mathbf{y}_i - \mathbf{y}_{i+1})\mathbf{m}_i(\mathbf{x})$, where $\sigma : \mathbb{R} \rightarrow \mathbb{R}$ is a positive function such that $\sigma(a) = 0$ only when $a = 0$, and \mathbf{m}_i is a strictly positive function. It is easy to verify that this parameterization of \mathbf{w} satisfies the requirements on \mathbf{w} in Theorem 1. However, we note that this class of functions cannot represent all possible \mathbf{w} stated in Theorem 1. In general, the speed $\mathbf{w}_i(\mathbf{x})$ converges to 0 can be a function of \mathbf{x} , but in the proposed factorization above, the rate of convergence to zero is a function of only two elements \mathbf{y}_i and \mathbf{y}_{i+1} . Fortunately, such a limitation does not substantially decrease the expressiveness of \mathbf{f} in practice, because the subspace where \mathbf{w}_i vanishes has zero measure in \mathbb{R}^n (i.e. subspaces where there is at least one tie in $\mathbf{x} \in \mathbb{R}^n$).

By Theorem 1 and Theorem 2, the proposed architecture in Fig. 3 ensures $\mathbf{f}(\mathbf{x})$ is continuous in \mathbf{x} as long as $\sigma(\mathbf{y}_i - \mathbf{y}_{i+1})$ and $\mathbf{m}_i(\mathbf{x})$ are continuous in \mathbf{x} . In the appendix, we show that this is true when σ and \mathbf{m}_i are continuous functions. Additionally, we prove that when σ and \mathbf{m} are continuously differentiable, $\mathbf{f}(\mathbf{x})$ is also directionally differentiable with respect to \mathbf{x} . Note that the differentiability to the input is not a requirement to learn the parameters of \mathbf{m} with a first order optimization algorithm which only needs \mathbf{f} to be differentiable with respect to the parameters of \mathbf{m} . The latter condition holds in general, since the only potential sources of non-differentiable \mathbf{f} , $S(\mathbf{x})^{-1}$ and \mathbf{y} are constant with respect to the parameters of \mathbf{m} . Thus, if \mathbf{m} is differentiable with respect to its parameters, \mathbf{f} is also differentiable with respect to the parameters of \mathbf{m} .

4 Implementation

Given a calibration dataset $\mathcal{D}_c = \{(\mathbf{z}^i, y^i)\}_{i=1}^N$ and a calibration function \mathbf{f} parameterized by some vector $\boldsymbol{\theta}$, we define the empirical calibration loss as $\frac{1}{N} \sum_{i=1}^N \ell(y^i, \mathbf{f}(\mathbf{x}^i)) + \frac{\lambda}{2} \|\boldsymbol{\theta}\|^2$, where $\mathbf{x}^i = \mathbf{g}(\mathbf{z}^i)$, $\ell : \mathcal{Y} \times \mathbb{R}^n \rightarrow \mathbb{R}$ is a classification cost function, and $\lambda \geq 0$ is the regularization weight. Here we follow the calibration literature [30, 7, 14] and use the negative log likelihood (NLL) loss, i.e., $\ell(y, \mathbf{f}(\mathbf{x})) = -\log(\mathbf{sm}_y(\mathbf{f}(\mathbf{x})))$, where \mathbf{sm} is the softmax operator and \mathbf{sm}_y is its y th element. We use the NLL loss in all the experiments to study the benefit of learning \mathbf{f} with different structures. The study of other loss functions for calibration [29, 33] is outside the scope of this paper.

To ensure \mathbf{f} is within the intra order-preserving family, we restrict \mathbf{f} to have the structure in Theorem 1 and set $\mathbf{w}_i(\mathbf{x}) = \sigma(\mathbf{y}_i - \mathbf{y}_{i+1})\mathbf{m}_i(\mathbf{x})$, as described in Section 3.4. We parameterize function \mathbf{m} by a generic multi-layer neural network and utilize the softplus activation $s^+(a) = \log(1 + \exp(a))$

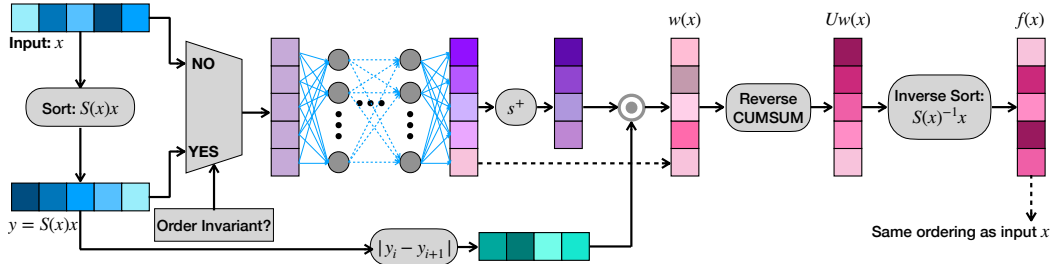


Figure 3: Flow graph of the intra order-preserving function. The vector $\mathbf{x} \in \mathbb{R}^n$ is the input to the graph. Function \mathbf{m} is estimated using a generic multi-layer neural network with non-linear activation for the hidden layers. The input to the network is sorted for learning order-preserving functions. We employ softplus activation function s^+ to impose strict positivity constraints.

on the last layer when strict positivity is desired and represent σ as $\sigma(a) = |a|$. For example, when $\mathbf{m}_i(\mathbf{x})$ is constant, our architecture recovers the temperature scaling scheme [7].

The order-invariant version in Theorem 2 can be constructed similarly. The only difference is that the neural network that parameterizes \mathbf{m} receives instead the sorted input. Fig. 3 illustrates the architecture of these models.

The diagonal intra order-preserving version in Theorem 3 is formed by learning an increasing function shared across all logit dimensions. We use the official implementation of proposed architecture in [31] that learns monotonic functions with unconstrained neural networks.

5 Related Work

Many different post-hoc calibration methods have been studied in the literature [27, 7, 14, 16, 15, 17]. Their main difference is in the parametric family of the calibration function. In Platt scaling [27], scale and shift parameters $a, b \in \mathbb{R}$ are used to transform the scalar logit output $x \in \mathbb{R}$ i.e. $f(x) = ax + b$ of a binary classifier. Temperature scaling [7] is a simple extension of Platt scaling for multi-class calibration in which only a single scalar temperature parameter is learned. Dirichlet calibration [14] allows learning within a richer linear functions family $f(\mathbf{x}) = W\mathbf{x} + \mathbf{b}$, where $W \in \mathbb{R}^{n \times n}$ and $\mathbf{b} \in \mathbb{R}^n$ but the learned calibration function may also change the decision boundary of the original model; Kull *et al.* [14] suggested regularizing the off-diagonal elements of W to avoid overfitting. Similar to our work, the concurrent work in Zhang *et al.* [39] also give special attention to order preserving transformations for calibration. However, their introduced functions are less expressive than the ones presented in this work. Earlier works like isotonic regression [36], histogram binning [35], and Bayesian binning [36] are also post-hoc calibration methods.

In contrast to post-hoc calibration methods, several researches proposed to modify the training process to learn a calibrated network in the first place. Data augmentation methods [30, 34] overcome overfitting by enriching the training data with new artificially generated pseudo data points and labels. Mixup [38] creates pseudo data points by computing the convex combination of randomly sampled pairs. Cutmix [34] uses a more efficient combination algorithm specifically designed for image classification in which two images are combined by overlaying a randomly cropped part of the first image on the second image. In label smoothing [26, 22], the training loss is augmented to penalize high confidence outputs. To discourage overconfident predictions, [29] modifies the original NLL loss by adding a cross-entropy loss term with respect to the uniform distribution. Similarly, [18] adds a calibration regularization to the NLL loss via kernel mean embedding.

Bayesian neural networks [5, 20] derive the uncertainty of the prediction by making stochastic perturbations of the original model. Notably, [5] uses dropout as approximate Bayesian inference. [20] estimates the posterior distribution over the parameters and uses samples from this distribution for Bayesian model averaging. These methods are computationally inefficient since they typically feed each sample to the network multiple times.

6 Experiments

We evaluate the performance of intra order-preserving (OP), order-invariant intra order-preserving (OI), and diagonal intra order-preserving (DIAG) families in calibrating the output of various im-

Table 1: ECE (with $M = 15$ bins) on various image classification datasets and models with different calibration methods. The subscript numbers represent the rank of the corresponding method on the given model/dataset. The accuracy of the uncalibrated model is shown in parentheses. The number in parentheses in DIR, MS, and UNCONSTRAINED methods show the change in accuracy for each method.

Dataset	Model	Uncal.	TS	DIR	MS	DIAG	OI	OP	UNCONSTRAINED
CIFAR10	ResNet 110	0.0475 ₈ (93.6%)	0.0113 ₅	0.0109 ₄ (-0.1%)	0.0106 ₃ (-0.1%)	0.0067 ₂	0.0061 ₁	0.0119 ₆	0.0170 ₇ (-0.4%)
CIFAR10	Wide ResNet 32	0.0451 ₈ (93.9%)	0.0078 ₄	0.0084 ₅ (+0.3%)	0.0073 ₂ (+0.3%)	0.0136 ₇	0.0064 ₁	0.0077 ₃	0.0097 ₆ (-0.1%)
CIFAR10	DenseNet 40	0.0550 ₈ (92.4%)	0.0095 ₂	0.0110 ₄ (+0.1%)	0.0099 ₃ (+0.1%)	0.0069 ₁	0.0116 ₅	0.0128 ₇	0.0125 ₆ (-0.5%)
SVHN	ResNet 152 (SD)	0.0086 ₈ (98.1%)	0.0061 ₅	0.0058 ₃ (+0.0%)	0.0060 ₄ (+0.0%)	0.0057 ₂	0.0116 ₆	0.0118 ₇	0.0015 ₁ (+0.0%)
CIFAR100	ResNet 110	0.1848 ₈ (71.5%)	0.0238 ₂	0.0282 ₅ (+0.2%)	0.0274 ₄ (+0.1%)	0.0507 ₇	0.0119 ₁	0.0253 ₃	0.0346 ₆ (-4.4%)
CIFAR100	Wide ResNet 32	0.1878 ₈ (73.8%)	0.0147 ₂	0.0189 ₅ (+0.1%)	0.0258 ₈ (+0.1%)	0.0172 ₃	0.0126 ₁	0.0173 ₄	0.0421 ₇ (-6.1%)
CIFAR100	DenseNet 40	0.2116 ₈ (70.0%)	0.0090 ₂	0.0114 ₄ (+0.1%)	0.0220 ₆ (+0.4%)	0.0075 ₁	0.0098 ₃	0.0154 ₅	0.0990 ₇ (-12.9%)
CARS	ResNet 50 (pre)	0.0239 ₇ (91.3%)	0.0144 ₃	0.0243 ₈ (+0.2%)	0.0186 ₆ (-0.3%)	0.0105 ₂	0.0103 ₁	0.0185 ₅	0.0182 ₄ (-3.5%)
CARS	ResNet 101 (pre)	0.0218 ₇ (92.2%)	0.0165 ₅	0.0225 ₈ (+0.0%)	0.0191 ₆ (-0.8%)	0.0102 ₁	0.0135 ₃	0.0125 ₂	0.0155 ₄ (-3.9%)
CARS	ResNet 101	0.0421 ₈ (85.2%)	0.0301 ₄	0.0245 ₃ (-0.3%)	0.0345 ₆ (-1.1%)	0.0206 ₁	0.0323 ₅	0.0358 ₇	0.0236 ₂ (-7.0%)
BIRDS	ResNet 50 (NTS)	0.0714 ₃ (87.4%)	0.0319 ₅	0.0486 ₆ (-0.2%)	0.0585 ₇ (-1.1%)	0.0188 ₂	0.0172 ₁	0.0292 ₄	0.0276 ₃ (-2.2%)
ImageNet	ResNet 152	0.0654 ₇ (76.2%)	0.0208 ₄	0.0452 ₅ (+0.1%)	0.0567 ₆ (+0.1%)	0.0087 ₁	0.0109 ₂	0.0167 ₃	0.1297 ₈ (-33.4%)
ImageNet	DenseNet 161	0.0572 ₇ (77.1%)	0.0198 ₄	0.0374 ₅ (+0.1%)	0.0443 ₆ (+0.4%)	0.0103 ₁	0.0123 ₂	0.0168 ₃	0.1380 ₈ (-28.1%)
ImageNet	PNASNet5 large	0.0610 ₇ (83.1%)	0.0713 ₈	0.0398 ₆ (+0.0%)	0.0217 ₄ (+0.3%)	0.0117 ₂	0.0084 ₁	0.0133 ₃	0.0316 ₅ (-4.8%)
Average Relative Error		1.00 ₈	0.42 ₄	0.49 ₅	0.50 ₆	0.27 ₁	0.33 ₂	0.41 ₃	0.66 ₇

age classification deep networks and compare their results with the previous post-hoc calibration techniques.

Datasets. We use six different datasets: CIFAR- $\{10,100\}$ [13], SVHN [24], CARS [12], BIRDS [32], and ImageNet [4]. In these datasets, the number of classes vary from 10 to 1000. We evaluate the performance of different post-hoc calibration methods to calibrate ResNet [8], Wide ResNet [37], DenseNet [9], and PNASNet5 [19] networks. We follow the experiment protocol in [14, 16] and use cross validation on the calibration dataset to find the best hyperparameters and architectures for all the methods. Please refer to the Appendix for detailed description of the datasets, pre-trained networks, and hyperparameter tuning.

Baselines. We compare the proposed function structures with temperature scaling (TS) [7], Dirichlet calibration with off-diagonal regularization (DIR) [14], and matrix scaling with off-diagonal regularization (MS) [14] as they are the current best performing post-hoc calibration methods. We also present the results of the original uncalibrated models (Uncal.) for comparison. To show the effect of intra order-preserving regularization, we also show the results of applying unconstrained multi-layer neural network without intra order-preserving constraint (UNCONSTRAINED). In cross-validation, we tune the architecture as well as regularization weight of UNCONSTRAINED and order-preserving functions. As we are using the same logits as [14], we report their results directly on CIFAR-10, CIFAR-100, and SVHN. However, since they do not present the results for CARS, BIRDS, and ImageNet datasets, we report the results of their official implementation³ on these datasets.

Results. Table 1 summarizes the results of our calibration methods and other baselines in terms of ECE and presents the average relative error with respect to the uncalibrated model. Overall, DIAG has the lowest average relative error followed by OI among the models and datasets presented in Table 1. OI is the best-performing method in 7 out of 14 experiments including ResNet 110 and Wide ResNet 32 models on CIFAR datasets as well as state-of-the-art PNASNet5 large model. DIAG family’s relative average error is half the MS and DIR methods and 15% less compared to Temp. Scaling. Although DIR and MS were able to maintain the accuracy of the original models in most of the cases by imposing off diagonal regularization, order-preserving family could significantly outperform them regarding the ECE metric. Finally, we remark that learning an unconstrained multi-layer neural network does not exhibit a good calibration performance and drastically hurts the accuracy in some datasets as shown in the last column of Table 1.

Fig. 4 illustrates the reliability diagrams of models trained on ResNet 152 (top row) and PNASNet5 large (bottom row). Weighted reliability diagrams are also presented to better indicate the differences regarding the ECE metric. Surprisingly, these diagrams show that the uncalibrated PNASNet5 large model is underconfident. The differences between the mappings learned by DIAG and temperature scaling on these models are illustrated on the right column. DIAG is capable of learning complex increasing functions while temperature scaling only scales all the logits. Compared with DIR and MS which learn a linear transformation, all intra order-preserving methods can learn non-linear transformations on the logits while decoupling accuracy from calibration of the predictions.

³https://github.com/dirichletcal/experiments_dnn/

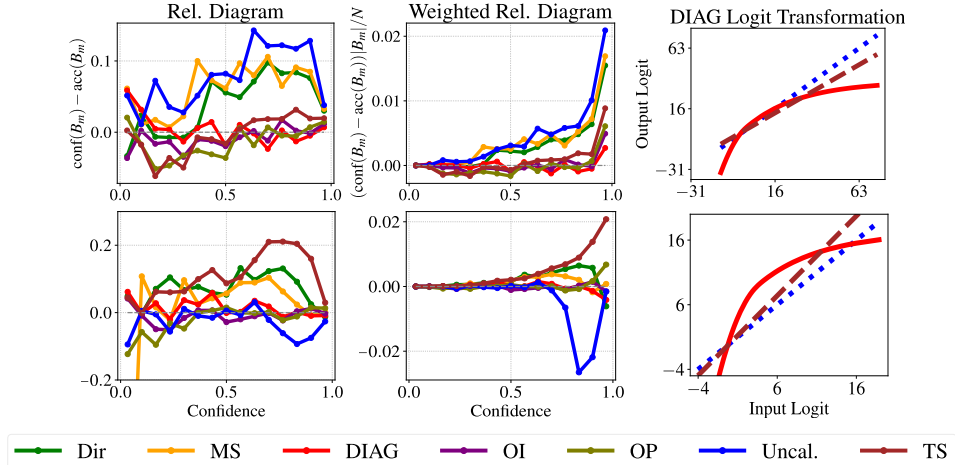


Figure 4: Performance evaluations of ResNet 152 (**Top Row**) and PNASNet5 large (**Bottom Row**) on ImageNet dataset. (**Left**) Reliability diagrams. As suggested by [20] we show the difference between the estimated confidence and accuracy over $M = 15$ bins. The dashed grey lines represent the perfectly calibrated network at $y = 0$. Points above (below) the grey line show overconfident (underconfident) predictions in a bin. (**Middle**) Weighted reliability diagrams where bin values are weighted by data frequency distribution. Since the uncalibrated network has different distances to the perfect calibration in different bins, scaling by a single temperature will lead to a mix of underconfident and overconfident regions. Our order-preserving functions, on the other hand, have more flexibility to reduce the calibration error. (**Right**) Transformation learned by DIAG function compared to temperature scaling and uncalibrated model (identity map).

In addition to ECE, which considers the top prediction, we also measure the NLL, Marginal Calibration Error [17], Classwise-ECE, and Brier score. As it is shown in Table 2, DIAG and OI have the best overall performance in terms of average relative error in most cases, while DIR is the top performing method in Classwise-ECE. Refer to the Appendix for discussions and the performance comparisons over all the datasets.

Table 2: Average relative error. Each entry shows the relative error compared to the uncalibrated model averaged over all the datasets. The subscripts represent the rank of the corresponding method on the given metric. See the Appendix for per dataset performance comparisons.

Evaluation Metric	Uncal.	TS	DIR	MS	DIAG	OI	OP
ECE	1.000 ₇	0.420 ₄	0.490 ₅	0.500 ₆	0.270 ₁	0.330 ₂	0.410 ₃
Debiased ECE [17]	1.000 ₇	0.357 ₃	0.430 ₆	0.409 ₅	0.213 ₁	0.337 ₂	0.406 ₄
NLL	1.000 ₇	0.766 ₄	0.772 ₆	0.768 ₅	0.749 ₁	0.751 ₂	0.765 ₃
Marginal Calibration Error [17]	1.000 ₇	0.750 ₃	0.735 ₂	0.996 ₆	0.725 ₁	0.778 ₄	0.898 ₅
Classwise-ECE	1.000 ₇	0.752 ₆	0.704 ₁	0.734 ₃	0.729 ₂	0.740 ₄	0.743 ₅
Brier	1.000 ₇	0.936 ₅	0.930 ₃	0.936 ₅	0.924 ₁	0.929 ₂	0.931 ₄

7 Conclusion

In this work, we introduce the family of intra order-preserving functions which retain the top- k predictions of any deep network when used as the post-hoc calibration function. We propose a new neural network architecture to represent these functions, and new regularization techniques based on order-invariant and diagonal structures. In short, calibrating neural network with this new family of functions generalizes many existing calibration techniques, with additional flexibility to express the post-hoc calibration function. The experimental results show the importance of learning within the intra order-preserving family as well as support the effectiveness of the proposed regularization in calibrating multiple classifiers on various datasets.

We believe the applications of intra order-preserving family are not limited to network calibration. Other promising domains include, e.g., data compression, depth perception system calibration, and tone-mapping in images where tone-maps need to be monotonic. Exploring the applicability of intra order-preserving functions in other applications is an interesting future direction.

Broader Impact

Predicting calibrated confidence scores for multi-class deep networks is important for avoiding rare but costly mistakes. Trusting the network’s output naively as confidence scores in system design could cause undesired consequences: a serious issue for applications where mistakes are costly, such as medical diagnosis, autonomous driving, suspicious events detection, or stock-market. As an example, in medical diagnosis, it is vital to estimate the chance of a patient being recovered by a certain operation given her/his condition. If the estimation is overconfident/underconfident this will put the life of the patient at risk. Confidence calibrated models would enable integration into downstream decision-making systems, allow machine learning interpretability, and help gain the user trust. While this work focuses primarily on some of the theoretical aspects of the neural network calibration, it also proposes novel techniques to potentially improve broader set of applications where preserving the rank of set of inputs is desired e.g. tone-mapping in images where tone-maps need to be monotonic, depth perception system calibration, and data compression.

We need to remark that our research shows that methods perform differently under various calibration metrics. Unfortunately, discrepancy between different calibration metrics is not well understood and fully explored in the literature. We believe more insights into these inconsistencies would be valuable to the field. We report the performance under different calibration metrics to highlight these differences for the future research. This also means that integrating the proposed work or any other calibration method into decision making systems requires application specific considerations. Other than that, since this work is mostly on the theoretical aspect of improving calibration, we do not foresee any direct negative impacts.

Acknowledgments and Disclosure of Funding

We would like to thank Antoine Wehenkel for providing helpful instructions for his unconstrained monotonic networks. This research is supported in part by the Australia Research Council Centre of Excellence for Robotics Vision (CE140100016).

References

- [1] Glenn W Brier. Verification of forecasts expressed in terms of probability. *Monthly weather review*, 78(1):1–3, 1950.
- [2] Zhe Cao, Tomas Simon, Shih-En Wei, and Yaser Sheikh. Realtime multi-person 2d pose estimation using part affinity fields. In *CVPR*, 2017.
- [3] Rich Caruana, Yin Lou, Johannes Gehrke, Paul Koch, Marc Sturm, and Noemie Elhadad. Intelligible models for healthcare: Predicting pneumonia risk and hospital 30-day readmission. In *ACM SIGKDD*, pages 1721–1730, 2015.
- [4] Jia Deng, Wei Dong, Richard Socher, Li-Jia Li, Kai Li, and Li Fei-Fei. Imagenet: A large-scale hierarchical image database. In *CVPR*, pages 248–255, 2009.
- [5] Yarín Gal and Zoubin Ghahramani. Dropout as a bayesian approximation: Representing model uncertainty in deep learning. In *ICML*, pages 1050–1059, 2016.
- [6] Ross Girshick. Fast r-cnn. In *ICCV*, pages 1440–1448, 2015.
- [7] Chuan Guo, Geoff Pleiss, Yu Sun, and Kilian Q Weinberger. On calibration of modern neural networks. In *ICML*, pages 1321–1330. JMLR. org, 2017.
- [8] Kaiming He, Xiangyu Zhang, Shaoqing Ren, and Jian Sun. Deep residual learning for image recognition. In *CVPR*, pages 770–778, 2016.
- [9] Gao Huang, Zhuang Liu, Laurens Van Der Maaten, and Kilian Q Weinberger. Densely connected convolutional networks. In *CVPR*, pages 4700–4708, 2017.
- [10] Xiaoqian Jiang, Melanie Osl, Jihoon Kim, and Lucila Ohno-Machado. Calibrating predictive model estimates to support personalized medicine. *Journal of the American Medical Informatics Association*, 19(2):263–274, 2012.
- [11] Alex Kendall and Yarín Gal. What uncertainties do we need in bayesian deep learning for computer vision? In *NeurIPS*, pages 5574–5584, 2017.

- [12] Jonathan Krause, Michael Stark, Jia Deng, and Li Fei-Fei. 3d object representations for fine-grained categorization. In *4th International IEEE Workshop on 3D Representation and Recognition (3dRR-13)*, Sydney, Australia, 2013.
- [13] Alex Krizhevsky, Geoffrey Hinton, et al. Learning multiple layers of features from tiny images. 2009.
- [14] Meelis Kull, Miquel Perello Nieto, Markus Kängsepp, Telmo Silva Filho, Hao Song, and Peter Flach. Beyond temperature scaling: Obtaining well-calibrated multi-class probabilities with Dirichlet calibration. In *NeurIPS*, pages 12295–12305, 2019.
- [15] Meelis Kull, Telmo Silva Filho, and Peter Flach. Beta calibration: a well-founded and easily implemented improvement on logistic calibration for binary classifiers. In *Artificial Intelligence and Statistics*, pages 623–631, 2017.
- [16] Meelis Kull, Telmo M Silva Filho, Peter Flach, et al. Beyond sigmoids: How to obtain well-calibrated probabilities from binary classifiers with beta calibration. *Electronic Journal of Statistics*, 11(2):5052–5080, 2017.
- [17] Ananya Kumar, Percy Liang, and Tengyu Ma. Verified uncertainty calibration. In *NeurIPS*, 2019.
- [18] Aviral Kumar, Sunita Sarawagi, and Ujjwal Jain. Trainable calibration measures for neural networks from kernel mean embeddings. In *ICML*, pages 2805–2814, 2018.
- [19] Chenxi Liu, Barret Zoph, Maxim Neumann, Jonathon Shlens, Wei Hua, Li-Jia Li, Li Fei-Fei, Alan L. Yuille, Jonathan Huang, and Kevin Murphy. Progressive neural architecture search. In *ECCV*, 2018.
- [20] Wesley J Maddox, Pavel Izmailov, Timur Garipov, Dmitry P Vetrov, and Andrew Gordon Wilson. A simple baseline for bayesian uncertainty in deep learning. In *NeurIPS*, pages 13132–13143, 2019.
- [21] Azadeh Sadat Mozafari, Hugo Siqueira Gomes, Wilson Leão, and Christian Gagné. Unsupervised temperature scaling: Post-processing unsupervised calibration of deep models decisions. 2019.
- [22] Rafael Müller, Simon Kornblith, and Geoffrey E Hinton. When does label smoothing help? In *NeurIPS*, pages 4696–4705, 2019.
- [23] Mahdi Pakdaman Naeini, Gregory Cooper, and Milos Hauskrecht. Obtaining well calibrated probabilities using bayesian binning. In *AAAI*, 2015.
- [24] Yuval Netzer, Tao Wang, Adam Coates, Alessandro Bissacco, Bo Wu, and Andrew Y Ng. Reading digits in natural images with unsupervised feature learning. 2011.
- [25] Jeremy Nixon, Mike Dusenberry, Linchuan Zhang, Ghassen Jerfel, and Dustin Tran. Measuring calibration in deep learning. *arXiv preprint arXiv:1904.01685*, 2019.
- [26] Gabriel Pereyra, George Tucker, Jan Chorowski, Łukasz Kaiser, and Geoffrey Hinton. Regularizing neural networks by penalizing confident output distributions. *arXiv preprint arXiv:1701.06548*, 2017.
- [27] John Platt. Probabilistic outputs for support vector machines and comparisons to regularized likelihood methods. *Advances in large margin classifiers*, 10(3):61–74, 1999.
- [28] Shaoqing Ren, Kaiming He, Ross Girshick, and Jian Sun. Faster r-cnn: Towards real-time object detection with region proposal networks. In *NeurIPS*, pages 91–99, 2015.
- [29] Seonguk Seo, Paul Hongsuck Seo, and Bohyung Han. Learning for single-shot confidence calibration in deep neural networks through stochastic inferences. In *CVPR*, pages 9030–9038, 2019.
- [30] Sunil Thulasidasan, Gopinath Chennupati, Jeff A Bilmes, Tanmoy Bhattacharya, and Sarah Michalak. On mixup training: Improved calibration and predictive uncertainty for deep neural networks. In *NeurIPS*, pages 13888–13899, 2019.
- [31] Antoine Wehenkel and Gilles Louppe. Unconstrained monotonic neural networks. In *NeurIPS*, pages 1543–1553, 2019.
- [32] Peter Welinder, Steve Branson, Takeshi Mita, Catherine Wah, Florian Schroff, Serge Belongie, and Pietro Perona. Caltech-UCSD Birds 200. Technical Report CNS-TR-2010-001, California Institute of Technology, 2010.

- [33] Chen Xing, Sercan Arik, Zizhao Zhang, and Tomas Pfister. Distance-based learning from errors for confidence calibration. In *ICLR*, 2020.
- [34] Sangdoon Yun, Dongyoon Han, Seong Joon Oh, Sanghyuk Chun, Junsuk Choe, and Youngjoon Yoo. Cutmix: Regularization strategy to train strong classifiers with localizable features. In *ICCV*, pages 6023–6032, 2019.
- [35] Bianca Zadrozny and Charles Elkan. Obtaining calibrated probability estimates from decision trees and naive bayesian classifiers. In *ICML*, volume 1, pages 609–616. Citeseer, 2001.
- [36] Bianca Zadrozny and Charles Elkan. Transforming classifier scores into accurate multiclass probability estimates. In *ACM SIGKDD*, pages 694–699, 2002.
- [37] Sergey Zagoruyko and Nikos Komodakis. Wide residual networks. In *BMVC*, 2016.
- [38] Hongyi Zhang, Moustapha Cissé, Yann N. Dauphin, and David Lopez-Paz. mixup: Beyond empirical risk minimization. In *ICLR*, 2018.
- [39] Jize Zhang, Bhavya Kailkhura, and T Han. Mix-n-match: Ensemble and compositional methods for uncertainty calibration in deep learning. In *ICML*, 2020.

A Missing Proofs

A.1 Proof of Theorem 1, Intra Order-preserving Functions

Theorem 1. *A continuous function $\mathbf{f} : \mathbb{R}^n \rightarrow \mathbb{R}^n$ is intra order-preserving, if and only if $\mathbf{f}(\mathbf{x}) = S(\mathbf{x})^{-1}U\mathbf{w}(\mathbf{x})$ with U being an upper-triangular matrix of ones and $\mathbf{w} : \mathbb{R}^n \rightarrow \mathbb{R}^n$ being a continuous function such that*

- $\mathbf{w}_i(\mathbf{x}) = 0$, if $\mathbf{y}_i = \mathbf{y}_{i+1}$ and $i < n$,
- $\mathbf{w}_i(\mathbf{x}) > 0$, if $\mathbf{y}_i > \mathbf{y}_{i+1}$ and $i < n$,
- $\mathbf{w}_n(\mathbf{x})$ is arbitrary,

where $\mathbf{y} = S(\mathbf{x})\mathbf{x}$ is the sorted version of \mathbf{x} .

Proof of Theorem 1. (\rightarrow) For a continuous intra order-preserving function $\mathbf{f}(\mathbf{x})$, let $\mathbf{w}(\mathbf{x}) = U^{-1}S(\mathbf{x})\mathbf{f}(\mathbf{x})$. First we show \mathbf{w} is continuous. Because \mathbf{f} is intra order-preserving, it holds that $S(\mathbf{x}) = S(\mathbf{f}(\mathbf{x}))$. Let $\hat{\mathbf{f}}(\mathbf{x}) := S(\mathbf{f}(\mathbf{x}))\mathbf{f}(\mathbf{x})$ be the sorted version of $\mathbf{f}(\mathbf{x})$. The above implies $\mathbf{w}(\mathbf{x}) = U^{-1}\hat{\mathbf{f}}(\mathbf{x})$. By Lemma 1, we know $\hat{\mathbf{f}}$ is continuous and therefore \mathbf{w} is also continuous.

Lemma 1. *Let $\mathbf{f} : \mathbb{R}^n \rightarrow \mathbb{R}^n$ be a continuous intra order-preserving function. $S(\mathbf{f}(\mathbf{x}))\mathbf{f}(\mathbf{x})$ is a continuous function.*

Next, we show that \mathbf{w} satisfies the properties listed in Theorem 1. As $\mathbf{w}(\mathbf{x}) = U^{-1}\hat{\mathbf{f}}(\mathbf{x})$, we can equivalently write \mathbf{w} as

$$\mathbf{w}_i(\mathbf{x}) = \begin{cases} \hat{\mathbf{f}}_i(\mathbf{x}) - \hat{\mathbf{f}}_{i+1}(\mathbf{x}) & 1 \leq i < n \\ \hat{\mathbf{f}}_n(\mathbf{x}) & i = n. \end{cases}$$

Since $\hat{\mathbf{f}}$ is the sorted version of \mathbf{f} , it holds that $\mathbf{w}_i(\mathbf{x}) \geq 0$ for $1 \leq i < n$. Also, by the definition of the order-preserving function, $\mathbf{w}_i(\mathbf{x})$ can be zero if and only if $\mathbf{y}_i = \mathbf{y}_{i+1}$, where $\mathbf{y} = S(\mathbf{x})\mathbf{x}$. These two arguments prove the necessary condition.

(\leftarrow) For a given $\mathbf{w}(\mathbf{x})$ satisfying the condition in the theorem statement, let $\mathbf{v}(\mathbf{x}) = U\mathbf{w}(\mathbf{x})$. Equivalently, we can write $\mathbf{v}_i(\mathbf{x}) = \sum_{j=0}^{n-i} \mathbf{w}_{n-j}(\mathbf{x})$ and $\mathbf{v}_i(\mathbf{x}) - \mathbf{v}_{i+1}(\mathbf{x}) = \mathbf{w}_i(\mathbf{x})$, $\forall i \in [n]$. By construction of \mathbf{w} , one can conclude that $\mathbf{v}(\mathbf{x})$ is a sorted vector where two consecutive elements $\mathbf{v}_i(\mathbf{x})$ and $\mathbf{v}_{i+1}(\mathbf{x})$ are equal if and only if $\mathbf{y}_i = \mathbf{y}_{i+1}$. Therefore, $\mathbf{f}(\mathbf{x}) = S(\mathbf{x})^{-1}\mathbf{v}(\mathbf{x})$ has the same ranking as \mathbf{x} . In other words, \mathbf{f} is an intra order-preserving function. The continuity of \mathbf{f} follows from the lemma below and the fact that \mathbf{v} is continuous when \mathbf{w} is continuous. Lemma 2.

Lemma 2. *Let $\mathbf{v} : \mathbb{R}^n \rightarrow \mathbb{R}^n$ be a continuous function in which $\mathbf{v}_i(\mathbf{x})$ and $\mathbf{v}_{i+1}(\mathbf{x})$ are equal if and only if $\mathbf{y}_i = \mathbf{y}_{i+1}$, where $\mathbf{y} = S(\mathbf{x})\mathbf{x}$. Then $\mathbf{f}(\mathbf{x}) = S(\mathbf{x})^{-1}\mathbf{v}(\mathbf{x})$ is a continuous function.*

■

A.1.1 Deferred Proofs of Lemmas

Proof of Lemma 1. Let $\mathbb{P}^n = \{P_1, \dots, P_K\}$ be the finite set of all possible $n \times n$ dimensional permutation matrices. For each $k \in [K]$, define the closed set $\mathbb{N}_k = \{\mathbf{x} : S(\mathbf{x})\mathbf{x} = P_k\mathbf{x}\}$. These sets are convex polyhedrons since each can be defined by a finite set of linear inequalities; in addition, they together form a covering set of \mathbb{R}^n . Note that $S(\mathbf{x}) = P_k$ is constant in the interior $\text{int}(\mathbb{N}_k)$, but $S(\mathbf{x})$ may change on the boundary $\partial(\mathbb{N}_k)$ which corresponds to points where a tie exists in elements of \mathbf{x} (for such a point $S(\mathbf{x}) \neq P_k$). Nonetheless, by definition of the set \mathbb{N}_k , we have $S(\mathbf{x})\mathbf{x} = P_k\mathbf{x}$ for all $\mathbf{x} \in \mathbb{N}_k$, which implies that $S(\mathbf{x})$ and P_k can only have different elements for indices where elements of \mathbf{x} are equal.

To prove that $\hat{\mathbf{f}}(\mathbf{x}) := S(\mathbf{f}(\mathbf{x}))\mathbf{f}(\mathbf{x})$ is continuous, we leverage the fact that $\hat{\mathbf{f}}(\mathbf{x}) = S(\mathbf{x})\mathbf{f}(\mathbf{x})$ for intra order-preserving \mathbf{f} . We will first show that $\hat{\mathbf{f}}(\mathbf{x}) = P_k\mathbf{f}(\mathbf{x})$ for $\mathbf{x} \in \mathbb{N}_k$ and any $k \in [K]$, which implies $\hat{\mathbf{f}}$ is continuous on \mathbb{N}_k when \mathbf{f} is continuous. To see this, consider an arbitrary $k \in [K]$. For

$\mathbf{x} \in \text{int}(\mathbb{N}_k)$ in the interior, we have $S(\mathbf{x}) = P_k$ and therefore $\hat{\mathbf{f}}(\mathbf{x}) = P_k \mathbf{f}(\mathbf{x})$. For $\mathbf{x} \in \partial\mathbb{N}_k$ on the boundary, we have

$$\hat{\mathbf{f}}(\mathbf{x}) = S(\mathbf{x})\mathbf{f}(\mathbf{x}) = P_k \mathbf{f}(\mathbf{x}).$$

The last equality holds because the difference between $S(\mathbf{x})$ and P_k are only in the indices for which elements of \mathbf{x} are equal, and the order-preserving \mathbf{f} preserves exactly the same equalities. Thus, the differences between permutations $S(\mathbf{x})$ and P_k do not reflect in the products $S(\mathbf{x})\mathbf{f}(\mathbf{x})$ and $P_k \mathbf{f}(\mathbf{x})$.

Next, we show that $\hat{\mathbf{f}}(\mathbf{x}) = P_k \mathbf{f}(\mathbf{x}) = P_{k'} \mathbf{f}(\mathbf{x})$ for $\mathbf{x} \in \partial\mathbb{N}_k \cap \partial\mathbb{N}_{k'}$. While $P_k \neq P_{k'}$, the intersection $\partial\mathbb{N}_k \cap \partial\mathbb{N}_{k'}$ contains exactly points \mathbf{x} such that the index differences in P_k and $P_{k'}$ correspond to same value in \mathbf{x} . Because \mathbf{f} is order-preserving, by an argument similar to the previous step, we have $P_k \mathbf{f}(\mathbf{x}) = P_{k'} \mathbf{f}(\mathbf{x})$ for $\mathbf{x} \in \partial\mathbb{N}_k \cap \partial\mathbb{N}_{k'}$.

Together these two steps and the fact that $\{\mathbb{N}_k\}$ is covering set on \mathbb{R}^n show that $\hat{\mathbf{f}}$ is a piece-wise continuous function on \mathbb{R}^n when \mathbf{f} is continuous on \mathbb{R}^n . ■

Proof of Lemma 2. In order to show the continuity of $\mathbf{f}(\mathbf{x})$, we use a similar argument as in Lemma 1 (see therein for notation definitions). For any $k \in [K]$, it is also trivial to show that \mathbf{f} is continuous over the open set $\text{int}(\mathbb{N}_k)$ since $\mathbf{f}(\mathbf{x}) = P_k^{-1} \mathbf{v}(\mathbf{x})$. We use the same argument as Lemma 1 to show it is also a continuous for any point $\mathbf{x} \in \partial(\mathbb{N}_k)$

$$\mathbf{f}(\mathbf{x}) = S(\mathbf{x})^{-1} \mathbf{v}(\mathbf{x}) = P_k^{-1} \mathbf{v}(\mathbf{x}).$$

The last equality holds because P_k^{-1} and $S(\mathbf{x})^{-1}$ can only have different elements among elements of $\mathbf{y} = S(\mathbf{x})\mathbf{x}$ with equal values, and \mathbf{v} preserves exactly these equalities in \mathbf{y} . Finally, the proof can be completed by piecing the results of different \mathbb{N}_k together. ■

A.2 Proof of Theorem 2, Order-invariant Functions

Theorem 2. *A continuous, intra order-preserving function $\mathbf{f} : \mathbb{R}^n \rightarrow \mathbb{R}^n$ is order-invariant, if and only if $\mathbf{f}(\mathbf{x}) = S(\mathbf{x})^{-1} U \mathbf{w}(\mathbf{y})$, where U , \mathbf{w} , and \mathbf{y} are in Theorem 1.*

To prove Theorem 2, we first study the properties of order invariant functions in Appendix A.2.1. We will provide necessary and sufficient conditions to describe order invariant functions, like what we did in Theorem 1 for intra order-preserving functions. Finally, we combine these insights and Theorem 1 to prove Theorem 2 in Appendix A.2.2.

A.2.1 Properties of Order Invariant Functions

The goal of this section is to prove the below theorem, which characterizes the representation of order invariant functions using the concept of equality-preserving.

Definition 6. We say a function $\mathbf{f} : \mathbb{R}^n \rightarrow \mathbb{R}^n$ is *equality-preserving*, if $\mathbf{f}_i(\mathbf{x}) = \mathbf{f}_j(\mathbf{x})$ for all $\mathbf{x} \in \mathbb{R}^n$ such that $\mathbf{x}_i = \mathbf{x}_j$ for some $i, j \in [n]$

Theorem 4. *A function $\mathbf{f} : \mathbb{R}^n \rightarrow \mathbb{R}^n$ is order-invariant, if and only if $\mathbf{f}(\mathbf{x}) = S(\mathbf{x})^{-1} \bar{\mathbf{f}}(S(\mathbf{x})\mathbf{x})$ for some function $\bar{\mathbf{f}} : \mathbb{R}^n \rightarrow \mathbb{R}^n$ that is equality-preserving on the domain $\{\mathbf{y} : \mathbf{y} = S(\mathbf{x})\mathbf{x}, \text{ for } \mathbf{x} \in \mathbb{R}^n\}$.*

Theorem 4 shows an order invariant function can be expressed in terms of some equality-preserving function. In fact, every order invariant function is equality-preserving.

Proposition 1. *Any order-invariant function $\mathbf{f} : \mathbb{R}^n \rightarrow \mathbb{R}^n$ is equality-preserving.*

Proof. Let $P_{ij} \in \mathbb{P}^n$ denote the permutation matrix that only swaps i^{th} and j^{th} elements of the input vector; i.e. $\mathbf{y} = P_{ij}\mathbf{x} \Rightarrow \mathbf{y}_i = \mathbf{x}_j, \mathbf{y}_j = \mathbf{x}_i, \mathbf{y}_k = \mathbf{x}_k, \forall \mathbf{x} \in \mathbb{R}^n, i, j, k \in [n]$, and $k \neq i, j$. Thus, for an order-invariant function $\mathbf{f} : \mathbb{R}^n \rightarrow \mathbb{R}^n$ and any $\mathbf{x} \in \mathbb{R}^n$ such that $\mathbf{x}_i = \mathbf{x}_j$, we have

$$\mathbf{f}(P_{ij}\mathbf{x}) = P_{ij}\mathbf{f}(\mathbf{x}) \Rightarrow \mathbf{f}_i(P_{ij}\mathbf{x}) = \mathbf{f}_j(\mathbf{x}) \Rightarrow \mathbf{f}_i(\mathbf{x}) = \mathbf{f}_j(\mathbf{x}) \quad (\because P_{ij}\mathbf{x} = \mathbf{x} \text{ for } \mathbf{x} \text{ such that } \mathbf{x}_i = \mathbf{x}_j).$$

We are almost ready to prove Theorem 4. We just need one more technical lemma, whose proof is deferred to the end of this section.

Lemma 3. For any $P \in \mathbb{P}^n$ and an equality-preserving $\mathbf{f} : \mathbb{R}^n \rightarrow \mathbb{R}^n$, $S(\mathbf{x})\mathbf{f}(\mathbf{x}) = S(P\mathbf{x})P\mathbf{f}(\mathbf{x})$.

Proof of Theorem 4. (\rightarrow) For an order-invariant function $\mathbf{f} : \mathbb{R}^n \rightarrow \mathbb{R}^n$, we have $\mathbf{f}(P\mathbf{x}) = P\mathbf{f}(\mathbf{x})$ by Definition 3 for any $P \in \mathbb{P}^n$. Take $P = S(\mathbf{x})$. We then have the equality $\mathbf{f}(\mathbf{x}) = S(\mathbf{x})^{-1}\mathbf{f}(S(\mathbf{x})\mathbf{x})$. This is an admissible representation because, by Proposition 1, \mathbf{f} is equality-preserving.

(\leftarrow) Let $\mathbf{f}(\mathbf{x}) = S(\mathbf{x})^{-1}\bar{\mathbf{f}}(S(\mathbf{x})\mathbf{x})$ for some equality-preserving function $\bar{\mathbf{f}}$. First, because $\bar{\mathbf{f}}$ is equality preserving and \mathbf{f} is constructed through the sorting function S , we notice that $\mathbf{f}(\mathbf{x})$ is equality-preserving. Next, we show \mathbf{f} is also order invariant:

$$\begin{aligned} \mathbf{f}(P\mathbf{x}) &= S(P\mathbf{x})^{-1}\bar{\mathbf{f}}(S(P\mathbf{x})P\mathbf{x}) \\ &= S(P\mathbf{x})^{-1}\bar{\mathbf{f}}(S(\mathbf{x})\mathbf{x}) && (\because S(P\mathbf{x})P\mathbf{x} = S(\mathbf{x})\mathbf{x} \text{ by choosing } \mathbf{f}(\mathbf{x}) = \mathbf{x} \text{ in Lemma 3}) \\ &= S(P\mathbf{x})^{-1}S(\mathbf{x})\mathbf{f}(\mathbf{x}) && (\because \text{definition of } \mathbf{f}(\mathbf{x})) \\ &= S(P\mathbf{x})^{-1}S(P\mathbf{x})P\mathbf{f}(\mathbf{x}) && (\because \text{Lemma 3}) \\ &= P\mathbf{f}(\mathbf{x}). \end{aligned}$$

■

A.2.2 Main Proof

Proof of Theorem 2. (\rightarrow) From Theorem 1 we can write $\mathbf{f}(\mathbf{x}) = S(\mathbf{x})^{-1}U\mathbf{w}(\mathbf{x})$. On the other hand, from Theorem 4 we can write $\mathbf{f}(\mathbf{x}) = S(\mathbf{x})^{-1}\bar{\mathbf{f}}(\mathbf{y})$ for some equality-preserving function $\bar{\mathbf{f}}$. Using both we can identify $\mathbf{w}(\mathbf{x}) = U^{-1}\bar{\mathbf{f}}(\mathbf{y})$ which implies that \mathbf{w} is only a function of the sorted input \mathbf{y} and can be equivalently written as $\mathbf{w}(\mathbf{y})$.

(\leftarrow) For \mathbf{w} with the properties in the theorem statement, the function $\mathbf{f}(\mathbf{x}) = S(\mathbf{x})^{-1}U\mathbf{w}(\mathbf{y})$ satisfies the conditions of Theorem 1; therefore \mathbf{f} is intra order-preserving. To show \mathbf{f} is also order-invariant, we write $\mathbf{f}(\mathbf{x}) = S(\mathbf{x})^{-1}\bar{\mathbf{f}}(\mathbf{y})$ where $\bar{\mathbf{f}}(\mathbf{y}) = U\mathbf{w}(\mathbf{y})$. Because $\bar{\mathbf{f}}_i(\mathbf{y}) = \sum_{j=0}^{n-i} \mathbf{w}_{n-j}(\mathbf{x})$, we can derive with the definition of \mathbf{w} that

$$\mathbf{y}_i = \mathbf{y}_{i+1} \Rightarrow \mathbf{w}_i(\mathbf{y}) = 0 \Rightarrow \bar{\mathbf{f}}_i(\mathbf{x}) = \bar{\mathbf{f}}_{i+1}(\mathbf{x}).$$

That is, $\bar{\mathbf{f}}(\mathbf{y})$ is equality-preserving on the domain of sorted inputs. Thus, \mathbf{f} is also order-invariant. ■

A.2.3 Deferred Proof of Lemmas

Proof of Lemma 3. To prove the statement, we first notice a fact that $S(\mathbf{x}) = S(P\mathbf{x})P$, for any $P \in \mathbb{P}^n$ and $\mathbf{x} \in \mathbb{X} := \{\mathbf{x} \in \mathbb{R}^n : \mathbf{x}_i \neq \mathbf{x}_j, \forall i, j \in [n], i \neq j\}$. Therefore, for $\mathbf{x} \in \mathbb{X}$, we have $S(\mathbf{x})\mathbf{f}(\mathbf{x}) = S(P\mathbf{x})P\mathbf{f}(\mathbf{x})$.

Otherwise, consider some $\mathbf{x} \in \mathbb{R}^n \setminus \mathbb{X}$. Without loss of generality⁴, we may consider $n > 2$ and \mathbf{x} such that $\mathbf{x}_1 = \mathbf{x}_2 > \mathbf{x}_k$ for all $k > 2$; because \mathbf{f} is equality-preserving, we have $\mathbf{f}_1(\mathbf{x}) = \mathbf{f}_2(\mathbf{x})$.

To prove the desired equality, we will introduce some extra notations. We use subscript $i:j$ to extract contiguous parts of a vector, e.g. $\mathbf{x}_{2:n} = [\mathbf{x}_2, \dots, \mathbf{x}_n]$ and $\mathbf{f}_{2:n}(\mathbf{x}) = [\mathbf{f}_2(\mathbf{x}), \dots, \mathbf{f}_n(\mathbf{x})]$ (by our construction of \mathbf{x} , $\mathbf{x}_{2:n}$ is a vector where each element is unique.) In addition, without loss of generality, suppose $P \in \mathbb{P}^n$ shifts index 1 to some index $i \in [n]$; we define $\bar{P} \in \{0, 1\}^{n-1 \times n-1}$ by removing the 1st column and the i th row of P (which is also a permutation matrix). Using this notion, we can partition $S(\bar{P}\mathbf{x}_{2:n}) \in \{0, 1\}^{n-1 \times n-1}$ as

$$S(\bar{P}\mathbf{x}_{2:n}) = \begin{bmatrix} B_1 & B_2 \\ B_3 & B_4 \end{bmatrix}$$

where $B_1 \in \mathbb{R}^{1 \times i-1}$, $B_2 \in \mathbb{R}^{1 \times n-i}$, $B_3 \in \mathbb{R}^{n-2 \times i-1}$, and $B_4 \in \mathbb{R}^{n-2 \times n-i}$. This would imply that $S(P\mathbf{x}) \in \{0, 1\}^{n \times n}$ can be written as one of followings

$$\begin{bmatrix} & e_i^\top & \\ B_1 & 0 & B_2 \\ B_3 & 0 & B_4 \end{bmatrix} \quad \text{or} \quad \begin{bmatrix} B_1 & 0 & B_2 \\ & e_i^\top & \\ B_3 & 0 & B_4 \end{bmatrix} \quad (1)$$

⁴This choice is only for convenience of writing the indices.

where e_i is the i th canonical basis.

To prove the statement, let $\mathbf{y} = P\mathbf{f}(\mathbf{x})$. By the definition of \bar{P} , we can also write \mathbf{y} as

$$\mathbf{y} = \begin{bmatrix} \mathbf{y}_{1:i-1} \\ \mathbf{y}_i \\ \mathbf{y}_{i+1:n} \end{bmatrix} = \begin{bmatrix} (\bar{P}\mathbf{f}_{2:n}(\mathbf{x}))_{1:i-1} \\ \mathbf{f}_1(\mathbf{x}) \\ (\bar{P}\mathbf{f}_{2:n}(\mathbf{x}))_{i:n-1} \end{bmatrix} \quad (2)$$

Let us consider the first case in (1). We have

$$S(P\mathbf{x})P\mathbf{f}(\mathbf{x}) = \begin{bmatrix} \mathbf{y}_i \\ B_1\mathbf{y}_{1:i-1} + B_2\mathbf{y}_{i+1:n} \\ B_3\mathbf{y}_{1:i-1} + B_4\mathbf{y}_{i+1:n} \end{bmatrix} = \begin{bmatrix} \mathbf{y}_i \\ S(\bar{P}\mathbf{x}_{2:n})\bar{P}\mathbf{f}_{2:n}(\mathbf{x}) \\ S(\mathbf{x}_{2:n})\mathbf{f}_{2:n}(\mathbf{x}) \end{bmatrix} = \begin{bmatrix} \mathbf{f}_1(\mathbf{x}) \\ S(\mathbf{x}_{2:n})\mathbf{f}_{2:n}(\mathbf{x}) \end{bmatrix} = S(\mathbf{x})\mathbf{f}(\mathbf{x})$$

where the second equality follows from (2), the third from the fact we proved at the beginning for the set \mathbb{X} , and the last equality is due to the assumption $\mathbf{x}_1 = \mathbf{x}_2 > \mathbf{x}_k$ and the equality-preserving property that $\mathbf{f}_1(\mathbf{x}) = \mathbf{f}_2(\mathbf{x})$. For the second case in (1), based on the same reasoning above, we can show

$$S(P\mathbf{x})P\mathbf{f}(\mathbf{x}) = \begin{bmatrix} (S(\mathbf{x}_{2:n})\mathbf{f}_{2:n}(\mathbf{x}))_1 \\ \mathbf{f}_1(\mathbf{x}) \\ (S(\mathbf{x}_{2:n})\mathbf{f}_{2:n}(\mathbf{x}))_{2:n-1} \end{bmatrix},$$

Because $\mathbf{x}_1 = \mathbf{x}_2$, we have $(S(\mathbf{x}_{2:n})\mathbf{f}_{2:n}(\mathbf{x}))_1 = \mathbf{f}_1(\mathbf{x}) = \mathbf{f}_2(\mathbf{x})$. Thus, $S(P\mathbf{x})P\mathbf{f}(\mathbf{x}) = S(\mathbf{x})\mathbf{x}$. ■

A.3 Proof of Theorem 3, Diagonal Functions

Theorem 3. *A continuous, intra order-preserving function $\mathbf{f} : \mathbb{R}^n \rightarrow \mathbb{R}^n$ is diagonal, if and only if $\mathbf{f}(\mathbf{x}) = [\bar{f}(\mathbf{x}_1), \dots, \bar{f}(\mathbf{x}_n)]$ for some continuous and increasing function $\bar{f} : \mathbb{R} \rightarrow \mathbb{R}$.*

We first prove some properties of *diagonal* intra order-preserving functions, which will be used to prove Theorem 3.

Proposition 2. *Any intra order-preserving function $\mathbf{f} : \mathbb{R}^n \rightarrow \mathbb{R}^n$ is equality-preserving.*

Proof. This can be seen directly from the definition of intra order-preserving functions. ■

Corollary 2. *The following statements are equivalent*

1. *A function $\mathbf{f} : \mathbb{R}^n \rightarrow \mathbb{R}^n$ is diagonal and equality-preserving.*
2. *$\mathbf{f}(\mathbf{x}) = [\bar{f}(\mathbf{x}_1), \dots, \bar{f}(\mathbf{x}_n)]$ for some $\bar{f} : \mathbb{R} \rightarrow \mathbb{R}$.*
3. *A function $\mathbf{f} : \mathbb{R}^n \rightarrow \mathbb{R}^n$ is diagonal and order-invariant.*

Proof. (1 \rightarrow 2) Let $\mathbf{f}(\mathbf{x}) = [f_1(\mathbf{x}_1), \dots, f_n(\mathbf{x}_n)]$ be a diagonal and equality-preserving function. One can conclude that $\mathbf{f}_1(x) = \dots = \mathbf{f}_n(x)$ for all $x \in \mathbb{R}$.

(2 \rightarrow 3) Let $\mathbf{u} = P\mathbf{x}$ for some permutation matrix $P \in \mathbb{P}^n$. Then $\mathbf{f}(P\mathbf{x}) = [\bar{f}(\mathbf{u}_1), \dots, \bar{f}(\mathbf{u}_n)] = P[\bar{f}(\mathbf{x}_1), \dots, \bar{f}(\mathbf{x}_n)] = P\mathbf{f}(\mathbf{x})$.

(3 \rightarrow 1) True by Proposition 1. ■

Proof of Theorem 3. (\rightarrow) By Proposition 2, an intra order-preserving function \mathbf{f} is also equality-preserving. Therefore, by Corollary 2 it can be represented in the form $\mathbf{f}(\mathbf{x}) = [\bar{f}(\mathbf{x}_1), \dots, \bar{f}(\mathbf{x}_n)]$ for some $\bar{f} : \mathbb{R} \rightarrow \mathbb{R}$. Furthermore, because $\mathbf{f}(\mathbf{x})$ is intra order-preserving, for any $\mathbf{x} \in \mathbb{R}^n$ with $\mathbf{x}_1 > \mathbf{x}_2$, it satisfies $\mathbf{f}_1(\mathbf{x}_1) > \mathbf{f}_2(\mathbf{x}_2)$; that is, $\bar{f}(\mathbf{x}_1) > \bar{f}(\mathbf{x}_2)$. Therefore, \bar{f} is an increasing function. Continuity is inherited naturally.

(\leftarrow) Because $\mathbf{f}_i(\mathbf{x}) = \bar{f}(\mathbf{x}_i)$ and \bar{f} is an increasing function, it follows that \mathbf{f} is intra order-preserving

$$\mathbf{x}_i = \mathbf{x}_j \Rightarrow \mathbf{f}_i(\mathbf{x}) = \mathbf{f}_j(\mathbf{x}) \quad \text{and} \quad \mathbf{x}_i > \mathbf{x}_j \Rightarrow \mathbf{f}_i(\mathbf{x}) > \mathbf{f}_j(\mathbf{x}).$$

■

Finally, we prove that diagonal intra order-preserving functions are also order-invariant. This fact was mentioned in the paper without a proof.

Corollary 3. *A diagonal intra order-preserving function is also order-invariant.*

Proof. Intra order-preserving functions are equality-preserving by Proposition 2. By Corollary 2 an diagonal equality-preserving function is order-invariant. ■

B Continuity and Differentiability of the Proposed Architecture

In this section, we discuss properties of the function $\mathbf{f}(\mathbf{x}) = S(\mathbf{x})^{-1}UD(\mathbf{y})\mathbf{m}(\mathbf{x})$. In order to learn the parameters of \mathbf{m} with a first order optimization algorithm, it is important for \mathbf{f} to be differentiable with respect to the parameters of \mathbf{m} . This condition holds in general, since the only potential sources of non-differentiable \mathbf{f} , $S(\mathbf{x})^{-1}$ and \mathbf{y} are constant with respect to the parameters of \mathbf{m} . Thus, if \mathbf{m} is differentiable with respect to its parameters, \mathbf{f} is also differentiable with respect to the parameters of \mathbf{m} .

Next, we discuss continuity and differentiability of $\mathbf{f}(\mathbf{x})$ with respect the *input* \mathbf{x} . These properties are important when the input to function f is first processed by a trainable function g (i.e. the final output is computed as $\mathbf{f} \circ \mathbf{g}(\mathbf{x})$). This is not the case in post-hoc calibration considered in the paper, since the classifier g here is not being trained in the calibration phase.

We show below that when $\mathbf{w}(\mathbf{x}) = D(\mathbf{y})\mathbf{m}(\mathbf{x})$ satisfies the requirements in Theorem 1, the function $\mathbf{f}(\mathbf{x}) = S(\mathbf{x})^{-1}UD(\mathbf{y})\mathbf{m}(\mathbf{x})$ is a continuous intra order-preserving function.

Corollary 4. *Let $\sigma : \mathbb{R} \rightarrow \mathbb{R}$ be a continuous function where $\sigma(0) = 0$ and strictly positive on $\mathbb{R} \setminus \{0\}$, and let \mathbf{m} be a continuous function where $\mathbf{m}_i(\mathbf{x}) > 0$ for $i < n$, and arbitrary for $\mathbf{m}_d(\mathbf{y})$. Let $D(\mathbf{y})$ denote a diagonal matrix with entries $D_{ii} = \sigma(\mathbf{y}_i - \mathbf{y}_{i+1})$ for $i < n$ and $D_{nn} = 1$. Then $\mathbf{w}(\mathbf{x}) = D(\mathbf{y})\mathbf{m}(\mathbf{x})$ is a continuous function and satisfies the following conditions*

- $\mathbf{w}_i(\mathbf{x}) = 0$, for $i < n$ and $\mathbf{y}_i = \mathbf{y}_{i+1}$
- $\mathbf{w}_i(\mathbf{x}) > 0$, for $i < n$ and $\mathbf{y}_i > \mathbf{y}_{i+1}$
- $\mathbf{w}_n(\mathbf{x})$ is arbitrary,

where $\mathbf{y} = S(\mathbf{x})\mathbf{x}$ is the sorted version of \mathbf{x} .

Proof. First, because $\mathbf{y} = S(\mathbf{x})\mathbf{x}$ is a continuous function (by Lemma 1 with $\mathbf{f}(\mathbf{x}) = \mathbf{x}$), $\mathbf{w}(\mathbf{x}) = D(\mathbf{y})\mathbf{m}(\mathbf{x})$ is also a continuous function. Second, because $\|\mathbf{x}\| < \infty$, we have $\mathbf{m}(\mathbf{x}) < \infty$ due to continuity. Therefore, it follows that $\mathbf{w}_i(\mathbf{x}) = \sigma(\mathbf{y}_i - \mathbf{y}_{i+1})\mathbf{m}_i(\mathbf{x})$ satisfies all the listed conditions. ■

To understand the differentiability of \mathbf{f} , we first see that \mathbf{f} may not be differentiable at a point where there is a tie among some elements of the input vector.

Corollary 5. *For \mathbf{w} in Corollary 4, there exists differentiable functions \mathbf{m} and σ such that $\mathbf{f}(\mathbf{x}) = S(\mathbf{x})^{-1}U\mathbf{w}(\mathbf{x})$ is not differentiable globally on \mathbb{R}^n .*

Proof. For the counter example, let $\mathbf{m} : \mathbb{R}^3 \rightarrow \mathbb{R}^3$ be a constant function $\mathbf{m}(\mathbf{x}) = [1, 1, 1]^\top$, and $\sigma(a) = a^2$. It is easy to verify that they both satisfy the conditions in Corollary 4 and are differentiable. We show that the partial derivative $\frac{\partial \mathbf{f}_1(\mathbf{x})}{\partial \mathbf{x}_3}$ does not exists at $\mathbf{x} = [2, 1, 1]^\top$. With few simple steps one could see $\mathbf{f}_1(\mathbf{x} + \alpha \mathbf{e}_3)$ for $\alpha \in (-\infty, 1]$ is

$$\mathbf{f}_1(\mathbf{x} + \alpha \mathbf{e}_3) = \begin{cases} \sigma(1) + \sigma(-\alpha) + 1 & \alpha \leq 0 \\ \sigma(1 - \alpha) + \sigma(\alpha) + 1 & 0 < \alpha \leq 1 \end{cases} \quad (3)$$

Though this function is continuous, the left and right derivatives are not equal at $\alpha = 0$ so the function is not differentiable at $\mathbf{x} = [2, 1, 1]^\top$. ■

The above example shows that \mathbf{f} may not be differentiable for tied inputs. On the other hand, it is straightforward to see function \mathbf{f} is differentiable at points where there is no tie. More precisely, for the points with tie in the input vector, we show the function \mathbf{f} is B-differentiable, which is a weaker condition than the usual (Frechét) differentiability.

Definition 7. [2] A function $\mathbf{f} : \mathbb{R}^n \rightarrow \mathbb{R}^m$ is said to be *B(ouligand)-differentiable* at a point $\mathbf{x} \in \mathbb{R}^n$, if \mathbf{f} is Lipschitz continuous in the neighborhood of \mathbf{x} and directionally differentiable at \mathbf{x} .

Proposition 3. For $\mathbf{f} : \mathbb{R}^n \rightarrow \mathbb{R}^m$ in Theorem 1, let $\mathbf{w}(\mathbf{x})$ be as defined in Corollary 4. If σ and \mathbf{m} are continuously differentiable, then \mathbf{f} is B-differentiable on \mathbb{R}^n .

Proof. Let $\mathbb{P}^n = \{P_1, \dots, P_K\}$ be the finite set of all possible $n \times n$ dimensional permutation matrices. For each $k \in [K]$, define the closed set $\mathbb{N}_k = \{\mathbf{x} : S(\mathbf{x})\mathbf{x} = P_k\mathbf{x}\}$. These sets are convex polyhedrons since each can be defined by a finite set of linear inequalities; in addition, they together form a covering set of \mathbb{R}^n .

If there is no tie in elements of vector \mathbf{x} , then $\mathbf{x} \in \text{int}(\mathbb{N}_k)$ for some $k \in [K]$. Since the sorting function $S(\mathbf{x})$ has the constant value P_k in a small enough neighborhood of \mathbf{x} , the function \mathbf{f} is continuously differentiable (and therefore B-differentiable) at \mathbf{x} .

Next we show that, for any point $\mathbf{x} \in \mathbb{R}^n$ with some tied elements, the directional derivative of \mathbf{f} along an arbitrary direction $\mathbf{d} \in \mathbb{R}^n$ exists. For such \mathbf{x} and \mathbf{d} , there exists a $k \in [K]$ and a small enough $\delta > 0$ such that $\mathbf{x}, \mathbf{x} + \epsilon\mathbf{d} \in \mathbb{N}_k$ for all $0 \leq \epsilon \leq \delta$. Therefore, we have $\mathbf{f}(\mathbf{x}') = \hat{\mathbf{f}}(\mathbf{x}')$ for all $\mathbf{x}' \in [\mathbf{x}, \mathbf{x} + \delta\mathbf{d}]$, where $\hat{\mathbf{f}}_k(\mathbf{x}) = P_k^{-1}UD(P_k\mathbf{x})\mathbf{m}(\mathbf{x})$. Let $\hat{\mathbf{f}}'_k(\mathbf{x}; \mathbf{d})$ denote the directional derivative of $\hat{\mathbf{f}}_k$ at \mathbf{x} along \mathbf{d} . By the equality of $\hat{\mathbf{f}}_k$ and \mathbf{f} in $[\mathbf{x}, \mathbf{x} + \delta\mathbf{d}]$, we conclude that the directional derivative $\mathbf{f}'(\mathbf{x}; \mathbf{d})$ exists and is equal to $\hat{\mathbf{f}}'_k(\mathbf{x}; \mathbf{d})$.

Finally, we note that \mathbf{f} is Lipschitz continuous, since it is composed by pieces of Lipschitz continuous functions $\hat{\mathbf{f}}_k$ for $k \in [K]$ (implied by the continuous differentiability assumption on σ and \mathbf{m}). Thus, \mathbf{f} is B-differentiable. ■

C Learning Increasing Functions

We follow the implementation of [10] for learning increasing functions in the diagonal subfamily. The idea is to learn an increasing function $\bar{f}(x) : \mathbb{R} \rightarrow \mathbb{R}$ using a neural network, which can be realized by learning a strictly positive function $\bar{f}'(x)$ and a bias $\bar{f}(0) \in \mathbb{R}$ and constructing the desired function \bar{f} by the integral $\bar{f}(x) = \int_0^x \bar{f}'(t)dt + \bar{f}(0)$. In implementation, the derivative \bar{f}' is modeled by a generic neural network and the positiveness is enforced by using a proper activation function in the last layer. In the forward computation, the integral is approximated numerically using Clenshaw-Curtis quadrature [1] and the backward pass is performed by Leibniz integral rule to reduce memory footprint. We use the official implementation of the algorithm provided by [10].

D Datasets, Hyperparameters, and Architecture Selection

The size of the calibration and the test datasets, as well as the number of classes for each dataset, are shown in Table 3. We note that the calibration sets sizes are the same as the previous methods [3, 5].

Table 3: Statistics of the Evaluation Datasets.

Dataset	#classes	Calibration set size	Test dataset size
CIFAR-10	10	5000	10000
SVHN	10	6000	26032
CIFAR-100	100	5000	10000
CARS	196	4020	4020
BIRDS	200	2897	2897
ImageNet	1000	25000	25000

Table 4: Hyperparameters learned by cross validation. For DIAG, OI, OP, and UNCONSTRAINED we show the network architectures learned by cross validation. The number of units in each layer are represented by a sequence of numbers, e.g. (10, 20, 30, 40) represents a network with 10 input units, 20 and 30 units in the first and second hidden layers, respectively, and 40 output units. We perform multi-fold cross-validation and select the architecture with lowest NLL on validation set.

Dataset	Model	DIAG	OI	OP	UNCONSTRAINED
CIFAR10	ResNet 110	(1,10,10,1)	(10,150,150,10)	(10,2,2,10)	(10,500,10)
CIFAR10	Wide ResNet 32	(1,2,2,1)	(10,10,10,10)	(10,2,2,10)	(10,150,150,10)
CIFAR10	DenseNet 40	(1,2,2,1)	(10,50,50,100)	(10,2,2,10)	(10,150,150,10)
SVHN	ResNet 152 (SD)	(1,20,20,1)	(10,10,10,10)	(10,50,50,10)	(10,500,10)
CIFAR100	ResNet 110	(1,10,10,1)	(100,100,100,100)	(100,150,150,100)	(100,500,100)
CIFAR100	Wide ResNet 32	(1,1,1)	(100,100,100,100)	(100,2,2,100)	(100,500,100)
CIFAR100	DenseNet 40	(1,1,1)	(100,10,10,100)	(100,2,2,100)	(100,500,500,100)
CARS	ResNet 50 (pre)	(1,50,1)	(196,10,196)	(196,2,2,196)	(196,500,196)
CARS	ResNet 101 (pre)	(1,20,20,1)	(196,100,100,196)	(196,20,20,196)	(196,500,196)
CARS	ResNet 101	(1,50,1)	(196,50,50,196)	(196,100,100,196)	(196,500,196)
BIRDS	ResNet 50 (NTS)	(1,50,50,1)	(200,150,150,200)	(200,50,50,200)	(200,500,200)
ImageNet	ResNet 152	(1,10,10,1)	(1000,150,150,1000)	(1000,2,2,1000)	(1000,150,1000)
ImageNet	DenseNet 161	(1,10,1)	(1000,100,100,1000)	(1000,2,2,1000)	(1000,150,1000)
ImageNet	PNASNet5 large	(1,20,20,1)	(1000,50,50,1000)	(1000,100,100,1000)	(1000,100,1000)

We follow the experiment protocol in [5] and use cross validation on the calibration set to find the best hyperparameters and architectures for all the methods. We found that [5] have improved their performance via averaging output predictions of models trained on different folds. We follow the same approach to have fair comparisons. Our criteria for selecting the best architecture is the NLL value. We perform 3 fold cross validation for ImageNet and 5 folds for all the other datasets. We limit our architecture to fully connected networks and vary the number of hidden layers as well as the size of each layer. We allow networks with up to 3 hidden layers in all the experiments. In CIFAR-10, SVHN, and CIFAR-100 with fewer classes, we test networks with {1, 2, 10, 20, 50, 100, 150} units per layer and for the larger CARS, BIRDS, and ImageNet datasets, we allow a wider range of {2, 10, 20, 50, 100, 150, 500} units per layer. We use the similar number of units for all the hidden layers to reduce the search space. We use ReLU activation for all middle hidden layers and Softplus on the last layer when strict positivity is desired. We utilize L-BFGS [7] for small scale optimization problems when the computational resources allow (temperature scaling and diagonal intra order-preserving (DIAG) methods on CIFAR and SVHN datasets) and use Adam [4] optimizer for other experiments. Table 4 summarize cross validation learned hyperparameter for each method.

Although the functions learned in Table 4 are more complicated than linear transformations used in the baselines, they are not too complex to slow down computation as the calibration network size is negligible compared to the backbone network used in the experiments. In our experiments, all methods take less than 0.5 milliseconds/sample in forward path and their differences are negligible.

We use the pre-computed logits of these networks provided by [5] for CIFAR, SVHN, and ImageNet with DenseNet and ResNet⁵. In addition, we use the publicly available state-of-the-art models for PNASNet5-large and ResNet50 NTSNet [11]⁶ for ImageNet and BIRDS datasets, respectively. Furthermore, we trained different ResNet type models on CARS dataset using the standard pytorch training script. The ResNet models with (pre) are initialized with pre-trained ImageNet weights. We will release these models for future research.

The effect of weight regularization on different metrics for MS and DIR methods is illustrated in Fig. 5. This shows that simply regularizing the off diagonal elements of a linear layer has limited expressiveness to achieve good calibration especially in the case that number of classes is large.

E More Experiments and Discussions

Reliability Diagrams. In Fig. 4 of the paper, we show the reliability diagrams and diagonal functions learned by TS and DIAG in ResNet 152 and PNASNet5 large on ImageNet dataset. Fig. 6 and 7 illustrate the reliability diagrams for different calibration algorithms in all the models. In general

⁵https://github.com/markus93/NN_Calibration

⁶<https://github.com/osmr/imgclsmb/blob/master/pytorch/README.md>

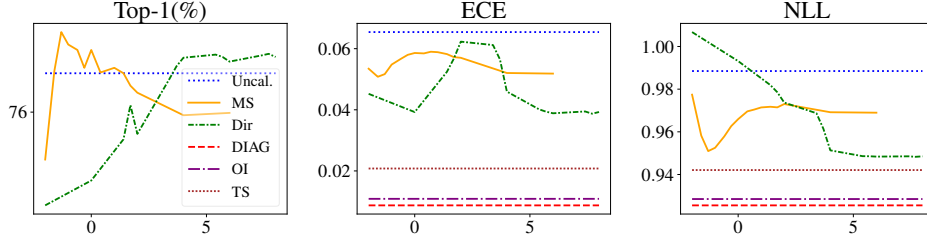


Figure 5: Accuracy, ECE, and NLL plots in MS and DIR for ResNet 152 on ImageNet with different regularization weights. In the plots, x-axis shows the log scale regularization and y-axis shows the accuracy, ECE, and NLL of different methods, respectively. The value of the bias regularizer is found by cross validation and kept constant for visualization purpose. Changing the bias regularizer has little effect on the final shape of the plots.

Table 5: Scores and rankings of different methods for Brier.

Dataset	Model	Uncal.	TS	DIR	MS	DIAG	OI	OP
CIFAR10	ResNet 110	0.01102 ₇	0.00979 ₆	0.00977 ₅	0.00976 ₄	0.00967 ₂	0.00963 ₁	0.00975 ₃
CIFAR10	Wide ResNet 32	0.01047 ₇	0.00924 ₄	0.00888 ₁	0.00889 ₂	0.00926 ₆	0.00921 ₃	0.00925 ₅
CIFAR10	DenseNet 40	0.01274 ₇	0.01100 ₄	0.01097 ₁	0.01097 ₁	0.01100 ₄	0.01110 ₆	0.01099 ₃
SVHN	ResNet 152 (SD)	0.00297 ₆	0.00291 ₁	0.00293 ₃	0.00298 ₇	0.00292 ₂	0.00293 ₃	0.00296 ₅
CIFAR100	ResNet 110	0.00453 ₇	0.00392 ₄	0.00391 ₃	0.00391 ₃	0.00393 ₅	0.00389 ₁	0.00390 ₂
CIFAR100	Wide ResNet 32	0.00432 ₇	0.00355 ₄	0.00354 ₂	0.00351 ₁	0.00355 ₄	0.00354 ₂	0.00355 ₄
CIFAR100	DenseNet 40	0.00491 ₇	0.00401 ₃	0.00400 ₁	0.00400 ₁	0.00401 ₃	0.00401 ₃	0.00402 ₆
CARS	ResNet 50 (pretrained)	0.000667 ₅	0.000666 ₄	0.000663 ₂	0.000679 ₇	0.000661 ₁	0.000664 ₃	0.000674 ₆
CARS	ResNet 101 (pretrained)	0.000620 ₆	0.000625 ₅	0.000623 ₃	0.000655 ₇	0.000622 ₂	0.000620 ₁	0.000623 ₃
CARS	ResNet 101	0.001131 ₆	0.001129 ₅	0.001123 ₃	0.001154 ₇	0.001118 ₁	0.001123 ₃	0.001119 ₂
BIRDS	ResNet 50 (NTSNet)	0.001035 ₆	0.000995 ₅	0.000988 ₄	0.001040 ₇	0.000977 ₃	0.000972 ₁	0.000974 ₂
ImageNet	ResNet 152	0.000338 ₇	0.000332 ₄	0.000333 ₆	0.000332 ₄	0.000329 ₁	0.000330 ₂	0.000331 ₃
ImageNet	DenseNet 161	0.000325 ₇	0.000321 ₄	0.000321 ₄	0.000318 ₁	0.000319 ₂	0.000320 ₃	0.000321 ₄
ImageNet	PNASNet5 large	0.000255 ₆	0.000261 ₇	0.000252 ₅	0.000247 ₃	0.000245 ₂	0.000244 ₁	0.000248 ₄
Average Relative Error		1.000 ₇	0.936 ₅	0.930 ₃	0.936 ₅	0.924 ₁	0.929 ₂	0.931 ₄

DIAG method outperforms other methods in calibration in most of the regions. OP and OI methods also achieve good calibration performance on this dataset and are slightly better than temperature scaling, while MS and DIR methods do not reduce the calibration error as much.

Calibration Set Size. In this experiment, we gradually increase the calibration set size from 10% to 100% of its original size to create smaller calibration subsets. Then, for each calibration subset, we train different post-hoc calibration methods and measure their accuracy, NLL, and ECE. The results are illustrated in Fig. 8. In overall, the performance of non intra order-preserving methods, i.e. DIR and MS, are more sensitive to the size of the calibration set while intra order-preserving methods maintain the accuracy and are more stable in terms of NLL and ECE.

Brier Score, NLL, and Classwise-ECE. As shown in Table 5, our OI is the best method in 5 out of 14 models with respect to the Brier score. MS also wins in 4 models. However, it performs poorly on CARS and BIRDS datasets. Our DIAG has the best average relative error. Overall, both OI and DIAG perform well on this metric. The DIR is the third best method on this metric and is slightly worse than OI in average relative error.

Results of different methods regarding the NLL metric are shown in Table 6. MS is the best method when the number of classes is less than or equal to 100 on this metric. Its performance degrades as the number of classes grows. This is typically due to the excessive number of parameters introduced by this method. Surprisingly, TS is the best method in SVHN with ResNet 152 (SD) model but its performance is very similar to the DIAG. The reason is that this model has a very high accuracy and the original model is actually already well calibrated. So, the single parameter TS would be enough to improve the calibration slightly. Our DIAG is the best method on datasets with larger number of classes and our OI is also comparable to it. Both these method have the best average ranking and DIAG has the best relative error on NLL.

Finally, Table 7 compares different methods in Classwise-ECE. While there is no single winning method on Classwise-ECE when the number of classes is less than 200, DIR is the best method on

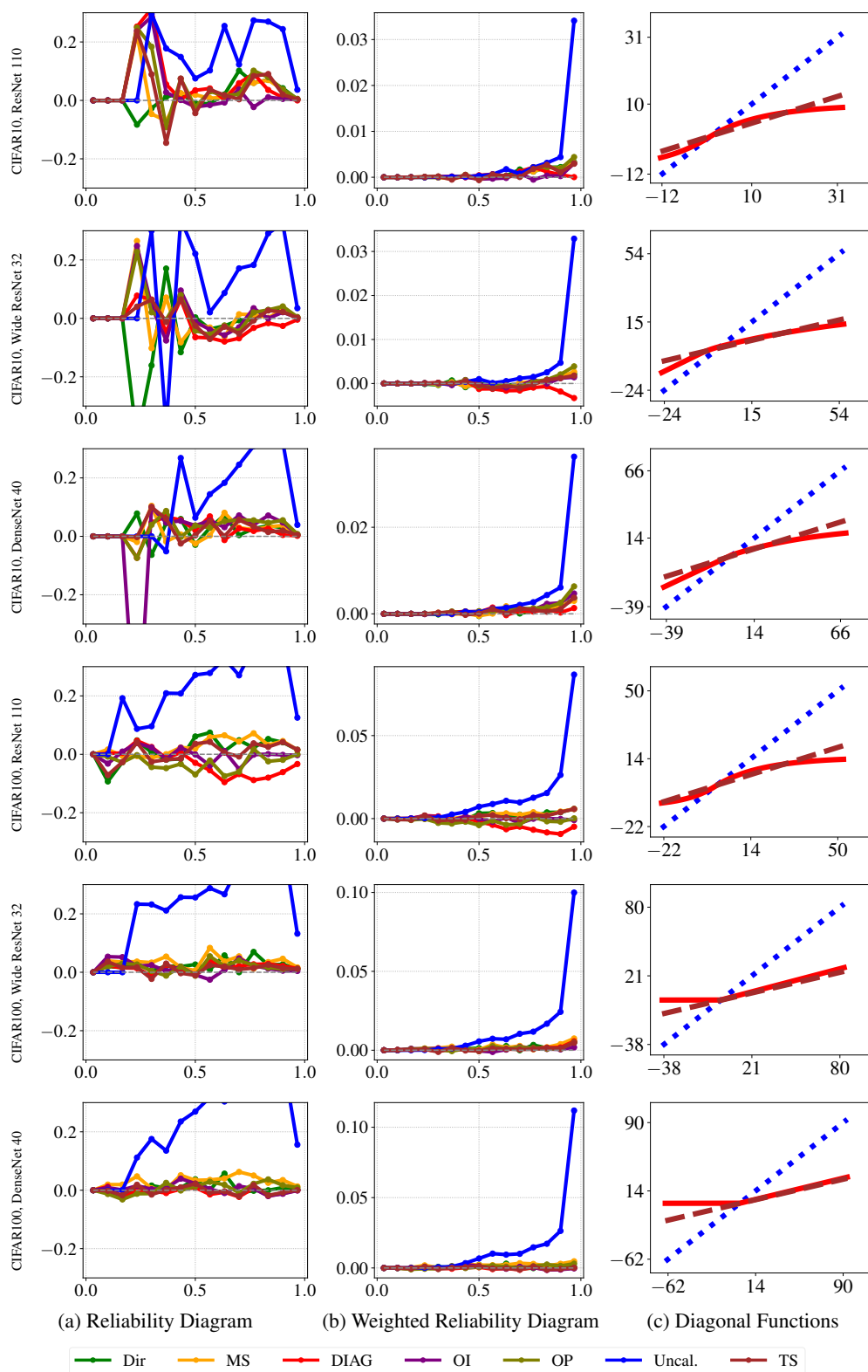


Figure 6: Reliability diagrams and learned diagonal functions. See Fig. 4 for the explanation of each diagram and axis.

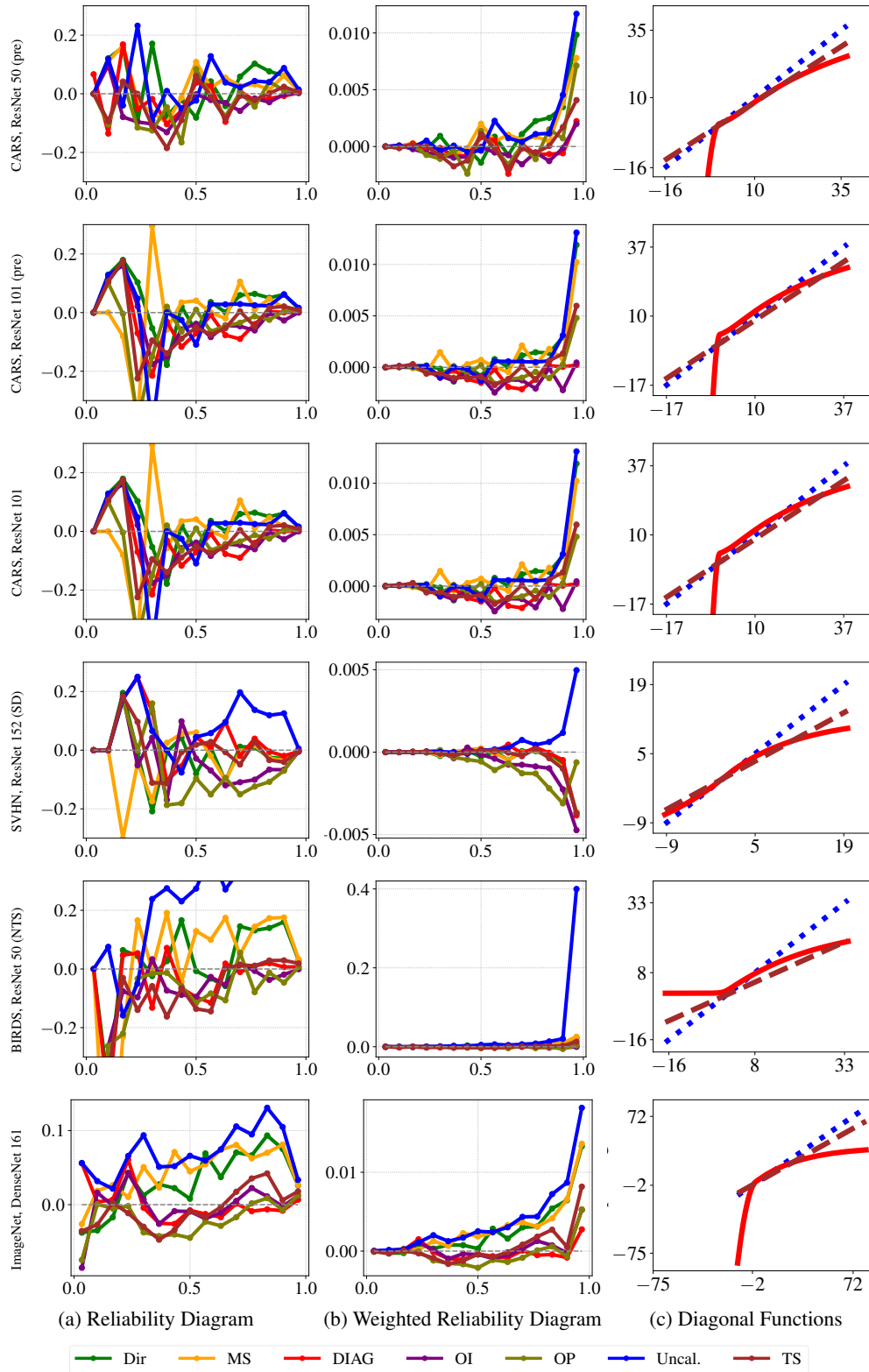


Figure 7: Reliability diagrams and learned diagonal functions. See Fig. 4 for the explanation of each diagram and axis.

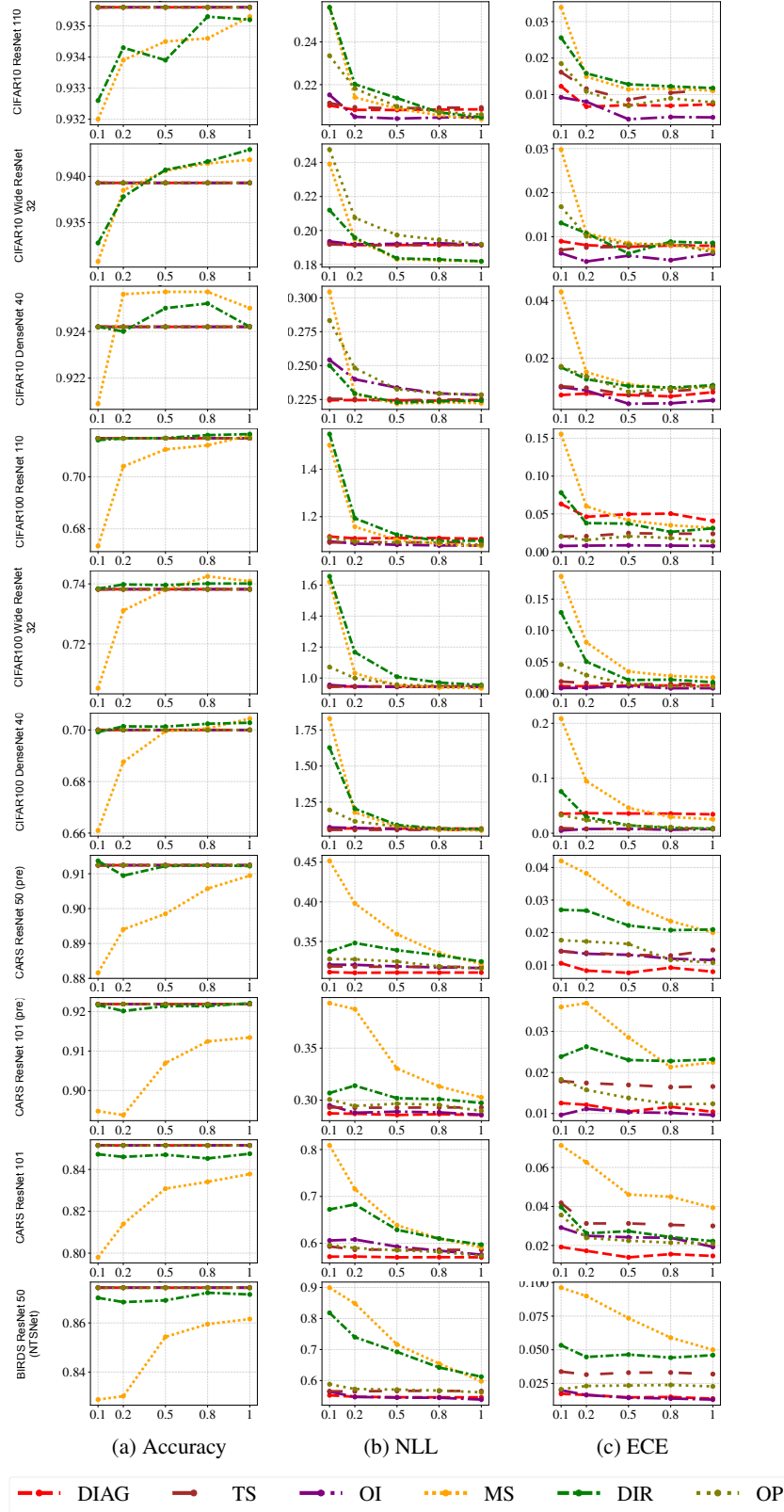


Figure 8: Accuracy, NLL, and ECE vs. calibration set size for CIFAR, CARS, BIRDS datasets. For each experiment, we use from 10% to 100% of the calibration set to train pos-hoc calibration functions and plot their accuracy, NLL, and ECE. Compared to DIR and MS, performance of the intra order-preserving methods (TS, DIAG, OI, and OP) degrades less with reducing the calibration set size.

Table 6: *NLL*.

Dataset	Model	Uncal.	TS	DIR	MS	DIAG	OI	OP
CIFAR10	ResNet 110	0.35827 ₇	0.20926 ₅	0.20511 ₃	0.20375 ₁	0.20674 ₄	0.20488 ₂	0.20954 ₆
CIFAR10	Wide ResNet 32	0.38170 ₇	0.19148 ₃	0.18203 ₂	0.18165 ₁	0.19221 ₅	0.19169 ₄	0.19332 ₆
CIFAR10	DenseNet 40	0.42821 ₇	0.22509 ₃	0.22371 ₂	0.22240 ₁	0.22551 ₄	0.23097 ₆	0.22798 ₅
SVHN	ResNet 152 (SD)	0.08542 ₇	0.07861 ₁	0.08038 ₅	0.08100 ₆	0.07887 ₂	0.07992 ₃	0.08010 ₄
CIFAR100	ResNet 110	1.69371 ₇	1.09169 ₄	1.09607 ₅	1.07370 ₁	1.10091 ₆	1.07966 ₂	1.08375 ₃
CIFAR100	Wide ResNet 32	1.80215 ₇	0.94453 ₃	0.95288 ₆	0.93273 ₁	0.94928 ₄	0.94312 ₂	0.95001 ₅
CIFAR100	DenseNet 40	2.01740 ₇	1.05713 ₂	1.05909 ₃	1.05084 ₁	1.05972 ₄	1.06127 ₅	1.07626 ₆
CARS	ResNet 50 (pretrained)	0.32993 ₇	0.31813 ₄	0.32381 ₆	0.31904 ₅	0.31234 ₁	0.31593 ₂	0.31793 ₃
CARS	ResNet 101 (pretrained)	0.30536 ₇	0.29329 ₃	0.29714 ₄	0.29788 ₅	0.28573 ₁	0.28897 ₂	0.30444 ₆
CARS	ResNet 101	0.61185 ₇	0.58619 ₄	0.59504 ₆	0.58683 ₅	0.57385 ₁	0.57774 ₂	0.58319 ₃
BIRDS	ResNet 50 (NTSNet)	0.74676 ₇	0.56569 ₄	0.61239 ₅	0.63055 ₆	0.54915 ₂	0.54508 ₁	0.56288 ₃
ImageNet	ResNet 152	0.98848 ₇	0.94208 ₄	0.95081 ₅	0.95786 ₆	0.92553 ₁	0.92850 ₂	0.93935 ₃
ImageNet	DenseNet 161	0.94397 ₇	0.90928 ₅	0.91214 ₆	0.90578 ₃	0.88937 ₁	0.89552 ₂	0.90632 ₄
ImageNet	PNASNet5 large	0.80240 ₇	0.75761 ₆	0.73955 ₅	0.71522 ₄	0.65550 ₁	0.65674 ₂	0.69593 ₃
Average Relative Error		1.000 ₇	0.766 ₄	0.772 ₆	0.768 ₅	0.749 ₁	0.751 ₂	0.765 ₃

Table 7: *Classwise ECE*.

Dataset	Model	Uncal.	TS	DIR	MS	DIAG	OI	OP
CIFAR10	ResNet 110	0.09846 ₇	0.04344 ₅	0.03950 ₄	0.03615 ₂	0.03791 ₃	0.03454 ₁	0.04435 ₆
CIFAR10	Wide ResNet 32	0.09530 ₇	0.04775 ₄	0.02947 ₂	0.02921 ₁	0.05462 ₆	0.04747 ₃	0.04918 ₅
CIFAR10	DenseNet 40	0.11430 ₇	0.03977 ₄	0.03687 ₂	0.03678 ₁	0.03877 ₃	0.04575 ₅	0.05182 ₆
SVHN	ResNet 152 (SD)	0.01940 ₄	0.01849 ₂	0.01988 ₅	0.02088 ₆	0.01478 ₁	0.01858 ₃	0.02128 ₇
CIFAR100	ResNet 110	0.41644 ₇	0.20095 ₃	0.18639 ₁	0.20270 ₅	0.21966 ₆	0.19977 ₂	0.20237 ₄
CIFAR100	Wide ResNet 32	0.42027 ₇	0.18573 ₄	0.17951 ₁	0.17966 ₂	0.18636 ₅	0.19397 ₆	0.18484 ₃
CIFAR100	DenseNet 40	0.47026 ₇	0.18664 ₃	0.18630 ₂	0.19112 ₅	0.18614 ₁	0.19866 ₆	0.18752 ₄
CARS	ResNet 50 (pretrained)	0.17353 ₃	0.18513 ₇	0.17094 ₂	0.18312 ₆	0.16891 ₁	0.18217 ₅	0.17567 ₄
CARS	ResNet 101 (pretrained)	0.16503 ₄	0.17186 ₆	0.15914 ₂	0.17405 ₇	0.16692 ₅	0.16434 ₃	0.15509 ₁
CARS	ResNet 101	0.26300 ₂	0.27234 ₆	0.26333 ₃	0.27447 ₇	0.26594 ₅	0.26488 ₄	0.25097 ₁
BIRDS	ResNet 50 (NTSNet)	0.24901 ₃	0.26369 ₇	0.22920 ₁	0.25639 ₆	0.25073 ₅	0.25069 ₄	0.24031 ₂
ImageNet	ResNet 152	0.31846 ₇	0.30884 ₆	0.30061 ₁	0.30895 ₅	0.31372 ₆	0.30642 ₃	0.30081 ₂
ImageNet	DenseNet 161	0.30992 ₇	0.30309 ₅	0.29403 ₁	0.29807 ₂	0.30659 ₆	0.30248 ₄	0.29959 ₃
ImageNet	PNASNet5 large	0.31356 ₇	0.25587 ₆	0.23797 ₁	0.24283 ₂	0.25004 ₅	0.24634 ₄	0.24493 ₃
Average Relative Error		1.000 ₇	0.752 ₆	0.704 ₁	0.734 ₃	0.729 ₂	0.740 ₄	0.743 ₅

this metric in ImageNet and in overall. In the next section, we discuss a hidden bias in Classwise-ECE metric that might become problematic. It seems Classwise-ECE might promote uncertainty in the output regardless of the actual accuracy of the model. This suggests there might be more investigation required for this metric and a practitioner should be cautious about these numbers.

E.1 Is Classwise-ECE a Proper Scoring Rule Calibration Metric?

It is known that ECE is not a proper scoring rule and thus there exist trivial solutions which yield optimal scores [9]. In this section, we show the same holds for Classwise-ECE metric. Classwise-ECE is “defined as the average gap across all classwise-reliability diagrams, weighted by the number of instances in each bin:

$$\text{Classwise-ECE} = \frac{1}{k} \sum_{j=1}^k \sum_{i=1}^m \frac{|B_{i,j}|}{n} |y_j(B_{i,j}) - \hat{p}_j(B_{i,j})| \quad (4)$$

where k , m , n are the numbers of classes, bins and instances, respectively, $|B_{i,j}|$ denotes the size of the bin, and $\hat{p}_j(B_{i,j})$ and $y_j(B_{i,j})$ denote the average prediction of class j probability and the actual proportion of class j in the bin $B_{i,j}$.” [5].

While the above definition of Classwise-ECE intuitively makes sense, we show that this metric fails to represent the quality of a predictor in a common degenerate case e.g. in a balanced dataset with k classes one could achieve a perfect Classwise-ECE by scaling down the logits with a large enough positive scalar. A large enough temperature value increases the uncertainty of the model and brings all the class probabilities close to $1/k$ while maintaining the accuracy of the model. As the result, in all the classwise-reliability diagrams every data point falls into the bin that contains confidence values around $1/k$. Since the dataset is balanced, the actual proportion of class j in that bin will also be $1/k$ so the model exhibits a perfect Classwise-ECE.

Table 8: *Temperature scaling effect on Classwise-ECE. A large temperature value improves the Classwise-ECE in most of the cases. The subscript numbers represent the rank compared to the values in Table 7. We remark that the purpose of this experiment is not to improve the performance but rather highlight the need for studying Classwise-ECE metric in the future works.*

Dataset	Model	Uncal.	Uncal./1000
CIFAR10	ResNet 110	0.09846	0.00021 ₁
CIFAR10	Wide ResNet 32	0.09530	0.00126 ₁
CIFAR10	DenseNet 40	0.11430	0.00143 ₁
SVHN	ResNet 152 (SD)	0.01940	0.33123 ₈
CIFAR100	ResNet 110	0.41644	0.00080 ₁
CIFAR100	Wide ResNet 32	0.42027	0.00199 ₁
CIFAR100	DenseNet 40	0.47026	0.00282 ₁
CARS	ResNet 50 (pretrained)	0.17353	0.16048 ₁
CARS	ResNet 101 (pretrained)	0.16503	0.16108 ₃
CARS	ResNet 101	0.26300	0.15067 ₁
BIRDS	ResNet 50 (NTSNet)	0.24901	0.05831 ₁
ImageNet	ResNet 152	0.31846	0.11074 ₁
ImageNet	DenseNet 161	0.30992	0.11074 ₁
ImageNet	PNASNet5 large	0.31356	0.10960 ₁

We remark that this problem does not happen with ECE, because ECE is computed with regard to the *accuracy* of the bins. While all the data points still fall inside the bin that contains the confidence value $1/k$, the accuracy of this bin would be equal to the accuracy of the model. Thus, there would be mismatch between the confidence and the accuracy of the bin, which results to a high ECE.

To validate this insight, we scale down the uncalibrated logit values by a large scalar number and see how it affects Classwise-ECE in Table 8. It shows this simple hack drastically improves the Classwise-ECE value of the uncalibrated models and outperforms the methods in Table 7 by large margin in most of the cases. Note that we can not achieve perfect Classwise-ECE because the datasets are not perfectly balanced.

We are concerned that this issue with *Classwise-ECE might bias future work to lean towards merely increasing the uncertainty of predictions without actually calibrating the model in a meaningful way.* To avoid this, Classwise-ECE metric should be always used with other proper scoring rule metrics (e.g., NLL or Brier) in evaluation. As we discuss in the next section, this issue would not happen when bins are dynamically chosen to ensure the number of data points in each bin remains equal.

E.2 Debiased ECE and a Fix to Classwise-ECE

We believe that the issue mentioned above is due to the binning scheme used in estimating Classwise-ECE which allows all the data points fall into a single bin. Nixon *et al.* [8] propose an adaptive binning scheme that guarantees the number of data points in each bin remains balanced; therefore, it does not exhibit the same issue as Classwise-ECE. In addition to the binning scheme, Kumar *et al.* [6] introduce *debiased ECE* and multiclass *marginal calibration error* metrics that are debiased versions similar to the ECE and Classwise-ECE metrics, respectively. The idea is to subtract an approximate correction term to reduce the biased estimate of the metrics. For the completeness, we present *debiased ECE* and multiclass *marginal calibration error* for all the methods in Table 9 and Table 10, respectively. While the results in debiased ECE are similar to ECE, comparing the results in Table 7 and Table 10 shows DIAG is performing better in terms of multiclass marginal calibration error and outperforms DIR in average relative error.

Overall, although the intra order-preserving models are the winning methods among most of the ever-increasing calibration metrics, one should carefully pick the calibration method and the metric depending on their application.

Table 9: *Debiased ECE [6].*

Dataset	Model	Uncal.	TS	DIR	MS	DIAG	OI	OP
CIFAR-10	ResNet 110	0.09070 ₇	0.01924 ₄	0.01927 ₅	0.01716 ₃	0.01573 ₂	0.00000 ₁	0.02282 ₆
CIFAR-10	Wide ResNet 32	0.08661 ₇	0.00809 ₂	0.00943 ₃	0.00958 ₄	0.01717 ₆	0.00194 ₁	0.01073 ₅
CIFAR-10	DenseNet 40	0.10340 ₇	0.01195 ₂	0.01228 ₃	0.01266 ₄	0.01130 ₁	0.02410 ₆	0.02309 ₅
SVHN	ResNet 152 (SD)	0.01922 ₅	0.00892 ₂	0.00979 ₄	0.00939 ₃	0.00617 ₁	0.02269 ₆	0.03429 ₇
CIFAR-100	ResNet 110	0.22699 ₇	0.02004 ₂	0.02842 ₃	0.03054 ₅	0.05596 ₆	0.00626 ₁	0.02903 ₄
CIFAR-100	Wide ResNet 32	0.24827 ₇	0.01031 ₂	0.01909 ₅	0.03018 ₆	0.01498 ₄	0.00545 ₁	0.01408 ₃
CIFAR-100	DenseNet 40	0.26523 ₇	0.00000 ₁	0.00000 ₁	0.02809 ₆	0.00000 ₁	0.00432 ₄	0.01265 ₅
CARS	ResNet 50 (pre)	0.02327 ₆	0.00900 ₂	0.02512 ₇	0.01605 ₄	0.00000 ₁	0.01611 ₅	0.01363 ₃
CARS	ResNet 101 (pre)	0.02181 ₆	0.01956 ₃	0.02419 ₇	0.01504 ₂	0.01964 ₄	0.02136 ₅	0.01271 ₁
CARS	ResNet 101	0.04280 ₅	0.02654 ₃	0.01518 ₁	0.03728 ₄	0.02542 ₂	0.04766 ₆	0.04821 ₇
BIRDS	ResNet 50 (NTS)	0.47117 ₇	0.04054 ₄	0.05545 ₅	0.07224 ₆	0.01518 ₁	0.01650 ₂	0.03104 ₃
ImageNet	ResNet 152	0.07745 ₇	0.02157 ₄	0.05247 ₅	0.06099 ₆	0.00066 ₁	0.00941 ₂	0.01804 ₃
ImageNet	DenseNet 161	0.06598 ₇	0.02008 ₄	0.04542 ₅	0.04888 ₆	0.00998 ₁	0.01158 ₂	0.01924 ₃
ImageNet	PNASNet5 large	0.06820 ₆	0.09620 ₇	0.05728 ₅	0.03580 ₄	0.01273 ₃	0.00713 ₁	0.01272 ₂
Average Relative Error		1.000 ₇	0.357 ₃	0.430 ₆	0.409 ₅	0.213 ₁	0.337 ₂	0.406 ₄

Table 10: *Marginal Calibration Error [6].*

Dataset	Model	Uncal.	TS	DIR	MS	DIAG	OI	OP
CIFAR-10	ResNet 110	0.00859 ₇	0.00305 ₂	0.00371 ₆	0.00363 ₅	0.00346 ₄	0.00218 ₁	0.00336 ₃
CIFAR-10	Wide ResNet 32	0.01516 ₇	0.01408 ₃	0.00410 ₁	0.00432 ₂	0.01442 ₆	0.01416 ₅	0.01410 ₄
CIFAR-10	DenseNet 40	0.01132 ₇	0.00602 ₄	0.00417 ₁	0.00583 ₂	0.00601 ₃	0.00729 ₆	0.00686 ₅
SVHN	ResNet 152 (SD)	0.00227 ₂	0.00245 ₃	0.00426 ₅	0.00541 ₆	0.00178 ₁	0.00387 ₄	0.00691 ₇
CIFAR-100	ResNet 110	0.00315 ₇	0.00129 ₁	0.00185 ₅	0.00233 ₆	0.00144 ₃	0.00141 ₂	0.00151 ₄
CIFAR-100	Wide ResNet 32	0.00356 ₇	0.00266 ₄	0.00222 ₂	0.00199 ₁	0.00270 ₆	0.00268 ₅	0.00257 ₃
CIFAR-100	DenseNet 40	0.00417 ₇	0.00266 ₆	0.00222 ₁	0.00263 ₅	0.00261 ₄	0.00259 ₃	0.00234 ₂
CARS	ResNet 50 (pre)	0.00063 ₆	0.00058 ₂	0.00035 ₁	0.00090 ₇	0.00060 ₅	0.00059 ₃	0.00059 ₃
CARS	ResNet 101 (pre)	0.00043 ₃	0.00044 ₄	0.00044 ₄	0.00092 ₇	0.00041 ₂	0.00034 ₁	0.00046 ₆
CARS	ResNet 101	0.00114 ₁	0.00114 ₁	0.00173 ₆	0.00230 ₇	0.00114 ₁	0.00118 ₅	0.00117 ₄
BIRDS	ResNet 50 (NTS)	0.00934 ₇	0.00139 ₄	0.00148 ₆	0.00141 ₅	0.00138 ₃	0.00132 ₂	0.00130 ₁
ImageNet	ResNet 152	0.00040 ₆	0.00038 ₂	0.00034 ₁	0.00042 ₇	0.00038 ₂	0.00038 ₂	0.00038 ₂
ImageNet	DenseNet 161	0.00041 ₇	0.00039 ₃	0.00035 ₁	0.00038 ₂	0.00039 ₃	0.00039 ₃	0.00039 ₃
ImageNet	PNASNet5 large	0.00039 ₇	0.00032 ₆	0.00025 ₁	0.00028 ₂	0.00028 ₂	0.00029 ₄	0.00030 ₅
Average Relative Error		1.000 ₇	0.750 ₃	0.735 ₂	0.996 ₆	0.725 ₁	0.778 ₄	0.898 ₅

References

- [1] Charles W Clenshaw and Alan R Curtis. A method for numerical integration on an automatic computer. *Numerische Mathematik*, 2(1):197–205, 1960.
- [2] Francisco Facchinei and Jong-Shi Pang. *Finite-dimensional variational inequalities and complementarity problems*. Springer Science & Business Media, 2007.
- [3] Chuan Guo, Geoff Pleiss, Yu Sun, and Kilian Q Weinberger. On calibration of modern neural networks. In *ICML*, pages 1321–1330. JMLR. org, 2017.
- [4] Diederik P Kingma and Jimmy Ba. Adam: A method for stochastic optimization. In *ICLR*, 2014.
- [5] Meelis Kull, Miquel Perello Nieto, Markus Kängsepp, Telmo Silva Filho, Hao Song, and Peter Flach. Beyond temperature scaling: Obtaining well-calibrated multi-class probabilities with Dirichlet calibration. In *NeurIPS*, pages 12295–12305, 2019.
- [6] Ananya Kumar, Percy Liang, and Tengyu Ma. Verified uncertainty calibration. In *NeurIPS*, 2019.
- [7] Dong C Liu and Jorge Nocedal. On the limited memory bfgs method for large scale optimization. *Mathematical programming*, 45(1-3):503–528, 1989.
- [8] Jeremy Nixon, Mike Dusenberry, Linchuan Zhang, Ghassen Jerfel, and Dustin Tran. Measuring calibration in deep learning. *arXiv preprint arXiv:1904.01685*, 2019.
- [9] Yaniv Ovadia, Emily Fertig, Jie Ren, Zachary Nado, David Sculley, Sebastian Nowozin, Joshua Dillon, Balaji Lakshminarayanan, and Jasper Snoek. Can you trust your model’s uncertainty? evaluating predictive uncertainty under dataset shift. In *NeurIPS*, 2019.
- [10] Antoine Wehenkel and Gilles Louppe. Unconstrained monotonic neural networks. In *NeurIPS*, pages 1543–1553, 2019.
- [11] Ze Yang, Tiange Luo, Dong Wang, Zhiqiang Hu, Jun Gao, and Liwei Wang. Learning to navigate for fine-grained classification. In *ECCV*, 2018.